Rectification and nonlinear transport in chaotic dots and rings

M. L. Polianski* and M. Büttiker
Département de Physique Théorique, Université de Genève, CH-1211 Genève 4, Switzerland
(Received 26 July 2007; revised manuscript received 20 September 2007; published 7 November 2007)

We investigate the nonlinear current-voltage characteristic of mesoscopic conductors and the current generated through rectification of an alternating external bias. To leading order in applied voltages both the nonlinear and the rectified current are quadratic. This current response can be described in terms of second order conductance coefficients and for a generic mesoscopic conductor they fluctuate randomly from sample to sample. Due to Coulomb interactions the symmetry of transport under magnetic field inversion is broken in a two-terminal setup. Therefore, we consider both the symmetric and antisymmetric nonlinear conductances separately. We treat interactions self-consistently taking into account nearby gates. The nonlinear current is determined by different combinations of second order conductances depending on the way external voltages are varied away from an equilibrium reference point (bias mode). We discuss the role of the bias mode and circuit asymmetry in recent experiments. In a photovoltaic experiment the alternating perturbations are rectified, and the fluctuations of the nonlinear conductance are shown to decrease with frequency. Their asymptotical behavior strongly depends on the bias mode and in general the antisymmetric conductance is suppressed stronger than the symmetric conductance. We next investigate nonlinear transport and rectification in chaotic rings. To this extent we develop a model which combines a chaotic quantum dot and a ballistic arm to enclose an Aharonov-Bohm flux. In the linear two-probe conductance the phase of the Aharonov-Bohm oscillation is pinned while in nonlinear transport phase rigidity is lost. We discuss the shape of the mesoscopic distribution of the phase and determine the phase fluctuations.

DOI: 10.1103/PhysRevB.76.205308 PACS number(s): 73.23.−b, 73.21.La, 73.40.Ei, 73.50.Fq

I. INTRODUCTION

A large part of modern physics is devoted to nonlinear classical and quantum phenomena in various systems. Such effects as the generation of the second harmonic or optical rectification are known from classical physics, while quantum electron pumping through a small sample due to interference of wave functions is a quantum nonlinear effect. Experiments on nonlinear electrical transport often combine classical and quantum contributions. A macroscopic sample without inversion center[1] exhibits a current-voltage characteristic which with increasing voltage departs from linearity due to terms proportional to the square of the applied voltage. If now an oscillating (ac) voltage is applied, a zero-frequency current (dc) is generated.

If the sample is sufficiently small, quantum effects can appear due to the wave nature of electrons. The uncontrollable distribution of impurities or small variations in the shape of the sample result in quantum contributions to the dc which are random. For a mesoscopic conductor with terminals $\alpha,\beta,\ldots$ we can describe the quadratic current response in terms of second order conductances $\mathcal{G}_{\alpha\beta\gamma}$. They relate voltages $V_{\beta,\omega}$ applied at contacts or neighboring gates β at frequency ω to the current at zero frequency at contact α,

$$I_\alpha = \sum_{\beta\gamma} \mathcal{G}_{\alpha\beta\gamma} |V_{\beta,\omega} - V_{\gamma,\omega}|^2. \tag{1}$$

The second order conductances include, in detail, the role of the shape and the nearby conductors (gates). They depend on external parameters like the frequency of the perturbation, temperature, magnetic field, or the connection of the sample to the environment.

We concentrate here on the quantum properties of nonlinear conductance through coherent chaotic samples. Chaos could result from the presence of impurities (disorder) or random scattering at the boundaries (ballistic billiard). Due to electronic interference the sign of this effect is generically random even for samples of macroscopically similar shape.[2–4] When averaged over an ensemble, the second order conductances vanish. As a consequence, for a fully chaotic sample there is no classical contribution to the dc and the nonlinear response is the result of the sample-specific quantum fluctuations.

Interestingly enough, from a fundamental point of view these fluctuations of nonlinear conductance are sensitive to the presence of Coulomb interactions and magnetic field. While interactions strongly affect the fluctuations' amplitude, their sign is easily changed by a small variation of magnetic flux Φ, similarly to universal conductance fluctuations (UCF) in linear transport. More importantly, without interactions the current (1) through a two-terminal sample is a symmetric function of magnetic field, just like linear conductance. However, the idea that Coulomb interactions are responsible for magnetic-field asymmetry in nonlinear current was recently proposed theoretically[5,6] and demonstrated experimentally in different mesoscopic systems.[7–12] (Various aspects of nonlinear quantum[13–16] and classical[17] charge and spin transport[18] have been discussed later on.) It is useful to consider (anti) symmetric second order conductance $\mathcal{G}_a, \mathcal{G}_s$ defined as

$$\begin{Bmatrix} \mathcal{G}_s(\Phi) \\ \mathcal{G}_a(\Phi) \end{Bmatrix} = \frac{h}{\nu_s e^3} \frac{\partial^2}{2\,\partial \tilde{V}^2} \left(\frac{I(\Phi) \pm I(-\Phi)}{2} \right)_{\tilde{V}\to 0}, \tag{2}$$

where $\tilde{V}$ is a combination of voltages at the gates and contacts varied in the experiment and ν_s accounts for the spin

degeneracy. We emphasize that, depending on the way voltages are varied, experiments probe different linear combinations of second order conductance elements $\mathcal{G}_{\alpha\beta\gamma}$ of Eq. (1). From now on we will simply call $\mathcal{G}_s, \mathcal{G}_a$ conductances and if no confusion is possible leave out the expression "second order."

In the presence of a dc perturbation the mesoscopic averages of antisymmetric[5,6] and symmetric[14,16] conductances vanish, and it is their sample-to-sample fluctuations that are measured. Experiments are usually performed for strongly interacting samples and the magnetic-field components $\mathcal{G}_s, \mathcal{G}_a$ allow one to evaluate the strength of interactions.[10,11] In previous theoretical works on nonlinear transport through chaotic dots several important issues have been discussed using random matrix theory (RMT).[5,14,16] Sánchez and Büttiker[5] found the fluctuations of $\mathcal{G}_a$ in a dot with arbitrary interaction strength at zero temperature and broken time-reversal symmetry due to magnetic field. Polianski and Büttiker considered the statistics of both $\mathcal{G}_a$ and $\mathcal{G}_s$ for arbitrary flux Φ, the temperature T, and the dephasing rate.[14] The fluctuations of relative asymmetry $\mathcal{A}=\mathcal{G}_a/\mathcal{G}_s$ and the role of the contact asymmetry on this quantity were discussed in Ref. 16. The results of the RMT approach were compared with experimental data of Zumbühl *et al.*[10] and Angers *et al.*[11]

Previously we considered statistics of $\mathcal{G}_a, \mathcal{G}_s$ for the dots where only one dc voltage was varied. However, to avoid parasitic circuit effects some experiments are performed varying several voltages simultaneously. Surprisingly, the importance of the chosen combination of varied voltages (bias mode) was not addressed before in the literature. It turns out that an experiment where only one of the voltages is varied[8,11,19] or two voltages are asymmetrically shifted[9,10] measure different combinations of nonlinear conductances $\mathcal{G}_{\alpha\beta\gamma}$. For example, in a weakly interacting dot in the first mode we found that $\mathcal{G}_s \gg \mathcal{G}_a$,[16] but in the second bias mode the fluctuations of nonlinear current are strongly reduced, so that $\mathcal{G}_s \sim \mathcal{G}_a$.

It is also important to generalize the previous treatment of the nonlinear current to mesoscopic systems biased by an ac voltage at *finite* frequency. The resulting dc is sometimes called "photovoltaic current." We expect that in such mesoscopic ac/dc converters the interactions lead to significant magnetic field-asymmetry in the dc signal. The rectification effect of mesoscopic diffusive metallic microjunctions was theoretically considered by Falko and Khmelnitskii[20] assuming that electrons do not interact. Therefore, a magnetic-field asymmetry was not predicted and was also not observed in subsequent experiments.[21–25] The fact that the interactions induce a magnetic field-asymmetry of the photovoltaic current when the size of the sample is strongly reduced was recently demonstrated in Aharonov-Bohm rings by Angers *et al.*[12]

However, it turns out that for an ac perturbation another quantum interference phenomenon, also quadratic in voltage, random in sign and magnetic field-asymmetric, contributes to the dc. Due to *internal* ac perturbations of the sample, the energy levels are randomly shifted and a phenomenon commonly referred to as "quantum pumping"[26,27] appears. Brouwer demonstrated that two voltages applied out of phase generate pumped current linear in frequency, while a single

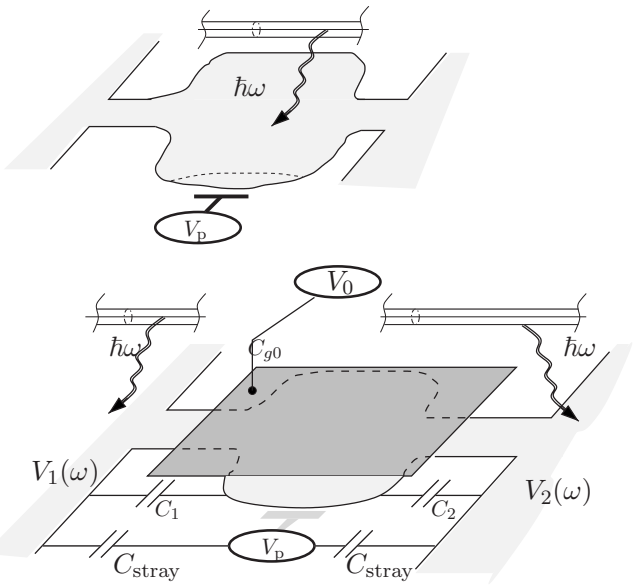

FIG. 1. Top: Quantum pumping sources include oscillating voltage $V_p(\omega)$ at the locally applied gate, which slightly changes the shape of the dot (shown dashed), or microwave antenna emitting photons with energy $\hbar\omega$ into the dot. Bottom: Rectification sources include external bias $V_{1,2}(\omega)$, top gate voltage $V_0(\omega)$ with capacitance C_{g0}, and parasitic coupling of $V_p(\omega)$ due to stray capacitances C_{stray}. Microwave antenna can emit photons to the contacts and lead not only to photon-assisted ac transport but also to a rectified dc.

voltage pumps current quadratic in frequency ω.[26] Although theory usually considers small (adiabatic) frequencies, a photovoltaic current could be induced by voltages applied at arbitrary frequency. At small ω the pumping contribution vanishes and only the rectification effect survives. In contrast, it is not clear what the ratio of pumping current to rectification current is at large ω. To distinguish between different mechanisms it is therefore important to consider rectification in a wide range of frequencies in detail.

We point here to a crucial difference between rectification and pumping contributions to the photovoltaic effect. Rectification results from external perturbations or the perturbations that can be reduced to the exterior by a gauge transformation. Typical examples are external ac bias, or gate voltage which shifts all levels uniformly,[28] or a bias induced by parasitic (stray) capacitance which connects sources of possible internal perturbations to macroscopic reservoirs;[29] see the bottom panel in Fig. 1. Pumping, on the other hand, is due to internal perturbations like those of a microwave antenna[30] or a locally applied gate voltage,[26] see the top panel in Fig. 1. Internal and external sources affect the Schrödinger equation and its boundary conditions, respectively. In experiment pumping and rectification, often considered together under the name of photovoltaic effect,[21–25,31] are hard to distinguish.

Can one clearly separate quantum pumping from rectification effects? To distinguish them it was proposed to use magnetic field asymmetry of dc as a signature of a true quantum pump effect. In Refs. 29 and 32 rectification by (noninteracting) quantum dot was due to stray capacitances of reservoirs with pumping sources. The rectified current was

found to be symmetric with respect to $\Phi \to -\Phi$.[29] While such field-symmetric rectification dominated in the experiments of Switkes *et al.*[33] and DiCarlo *et al.*[32] at MHz frequencies, an asymmetry $\Phi \to -\Phi$ observed at larger GHz frequencies seemed to signify a quantum pump effect.[32] It was noted that the Coulomb interactions treated self-consistently do not lead to any drastic changes in the mesoscopic distribution of a pumped current.[26] Probably, that is why the effect of interactions on the rectification have not been considered yet, even though the Coulomb interaction in such dots is known to be strong.[10]

However, as it turned out later, Coulomb interactions are responsible for magnetic-field asymmetry in nonlinear transport through quantum dots.[5] Similarly this could be expected for rectification as well. Then the magnetic field asymmetry alone can not safely distinguish pumping from rectification. Therefore we thoroughly examine the frequency dependence of the magnetic-field (anti)symmetric conductances $\mathcal{G}_a, \mathcal{G}_s$. Here we neglect any quantum pumping effects and their interference with rectification.[34,35] While the role of Coulomb interactions and the full frequency dependence in quantum pumping are yet to be explored, here we answer two important questions concerning a competing mechanism, rectification: (1) In the dc limit $\omega \to 0$ for a strongly interacting quantum dot $\mathcal{G}_a$ and $\mathcal{G}_s$ are of the same order. Is this also the case at finite frequencies? (2) How are the experimental data affected by the bias mode for alternating voltages?

A number of very recent experiments on nonlinear dc transport[9,11] and ac rectification[12] have used submicron ring-shaped samples with a relatively large aspect ratio. In this work we develop a model of a ring which includes chaotic dynamics due to possible roughness of its boundary and/or the presence of impurities. Similarly to quantum dots, the two-terminal nonlinear conductance of such a ring is field-asymmetric because field-asymmetry exists in each arm. In particular, this leads to deviations of the phase in AB oscillations from $0(\mathrm{mod})\pi$ which characterizes linear conductance obeying Onsager symmetry relations. Experiments find that the amplitude and phase of AB oscillations exhibit rather curious properties. For example, the dc experiment of Leturcq *et al.* [9] finds that during many AB oscillations with period hc/e the phase is well-defined. The experiment demonstrates that a nearby gate can vary the phase of the AB oscillations over the full circle. The amplitude of the second harmonic $hc/2e$ is strongly suppressed. On the other hand, the dc experiment[11] and ac experiment[12] of Angers *et al.* find that the phase can be defined only for few oscillations at low magnetic fields. For high frequencies, the phase fluctuates strongly as function of frequency. Both in the nonlinear and the rectified current the amplitude of the second harmonic $hc/2e$ in AB oscillations is always comparable with the first harmonic hc/e. This is in contrast with the experiments in Ref. 9. Although we do not fully address all these questions here, our model of a chaotic ring allows us to consider them at least on a qualitative level.

II. PRINCIPAL RESULTS

To introduce the reader to the problem of nonlinear transport in Sec. IV we first qualitatively discuss the Coulomb interaction effect in the simplest dc problem. In reality the statistical properties of conductances $\mathcal{G}_{\alpha\beta\gamma}$ in Eq. (1) are sensitive to electronic interference but to assess the role of Coulomb interactions we can consider a specific sample. In contrast to linear transport, it turns out that the nonlinear current strongly depends on the way voltages at the contacts and/or nearby conductors are varied from their equilibrium values (bias mode). For example, we find that the experiments when only one voltage at the contact is varied[8,11,19] or when two contact voltages are shifted oppositely[9,10] measure different nonlinear currents. Indeed, for a current $I(\{V_i\})$, bilinear in voltages, its second derivative should depend on the chosen direction in the space of voltages $\{V_i\}$. Interestingly, a sample with weak interactions is very sensitive to the choice of the bias mode, which we attribute to the strong effect of capacitive coupling of the sample with nearby conductors.

To make our arguments quantitative and consider the role of magnetic flux Φ for a quantum dot which is (generally) ac-biased at arbitrary frequency ω, in Sec. V we take electronic interference into account. Having done that, we illustrate the interplay between interactions and interference on several important examples. First, we consider nonlinear transport due to a constant applied voltage and then consider rectification of ac voltages.

For a two-terminal dot, in a generally asymmetric circuit (capacitive couplings included), in Sec. V A we find the statistics of (anti) symmetric conductances $\mathcal{G}_a, \mathcal{G}_s$ defined in Eq. (2). Both $\mathcal{G}_a$ and $\mathcal{G}_s$ vanish on average. Quantum fluctuations of $\mathcal{G}_s$ strongly depend on the interaction strength, circuit asymmetry and bias mode. This is in accordance with our qualitative picture. On the other hand, the antisymmetric component $\mathcal{G}_a$ depends only on interactions. Our arguments agree with recent experiments in quantum dots:[10,19] depending on the bias mode different features of the nonlinear conductance tensor are probed. The fluctuations of nonlinear current can be minimized or maximized (on average), which becomes important for weakly interacting electrons. Curiously, for symmetric coupling (transmission and capacitance) of contacts and dot the bias mode in which the voltages at the contacts are changed in opposite directions generally *minimizes* fluctuations of $\mathcal{G}_s$. Consequently, such a mode is more advantageous for the observation of $\mathcal{G}_a$ or a cleaner linear signal. Near the end of Sec. V A we also demonstrate how to take into account possible classical circuit-induced asymmetry[19] due to the finite classical resistance of the wires.

In Sec. V B we present results elucidating the role of interaction in rectification through two-terminal dots. Usually there are two important time scales: The dwell time τ_d an electron spends inside the dot and the charge relaxation time $\tau_{\mathrm{RC}} \leq \tau_d$ of the dot. For a given geometry, the dwell time depends on the coupling of the dot with reservoirs, but the charge relaxation time is also sensitive to the interaction strength. We have $\tau_{\mathrm{RC}} \ll \tau_d$ for strong interactions and $\tau_{\mathrm{RC}} = \tau_d$ in the weak interaction limit. Our results for fluctuations of $\mathcal{G}_a(\omega), \mathcal{G}_s(\omega)$ are obtained for arbitrary frequency ω. Although the fluctuations of both $\mathcal{G}_a(\omega)$ and $\mathcal{G}_s(\omega)$ monotonically decrease when $\omega \to \infty$, as functions of frequency ω they behave differently. At nonadiabatic frequencies $\omega\tau_d \gg 1$ the nearby gate short-circuits currents. This effect is even in

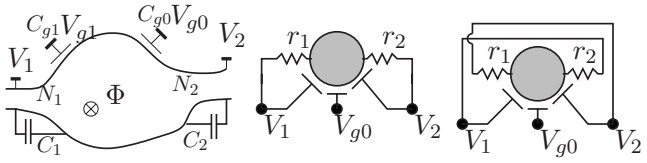

FIG. 2. (Left) Rectified current is measured through a coherent quantum dot biased by voltages with (ac) amplitude $V_{i,\omega}, i=1,2$ at reservoirs connected by N_i ballistic channels and capacitances C_i and by voltages $V_{gi,\omega}$ applied at additional gates with capacitances C_{gi}. Transport through the dot is sensitive to the total magnetic flux Φ through the area of the dot. (Center and right) Forward and reverse connection of Ref. 19 exchange voltages at the contacts and classical resistors $r_{1,2}$.

magnetic field and thus affects only $\mathcal{G}_s$. As a result, for a high-frequency voltage the asymptotes of $\mathcal{G}_a$ and $\mathcal{G}_s$ are generally different and strongly depend on the bias mode. Since the regime of parameters is quite realistic, we expect that the predicted difference of $\mathcal{G}_s(\omega)$ and $\mathcal{G}_a(\omega)$ should be experimentally observable. In the noninteracting limit our results qualitatively agree with those in diffusive metallic junctions.

Our model of a ring consisting of a chaotic dot with a ballistic arm which encloses an AB flux is presented in Sec. VI. Although it is impossible to find the full mesoscopic distribution of the AB phase δ, its shape can be discussed qualitatively. Since $\tan\delta$ is similar to the asymmetry parameter $\mathcal{A}=\mathcal{G}_a/\mathcal{G}_s$ in quantum dots, its distribution can become very wide for a particular choice of the bias mode. On average $\langle\delta(\mathrm{mod})\pi\rangle=0$ in our model, and we find the dependence of the fluctuations of δ on temperature, interactions, and number of channels of the contacts and the arm. Our treatment allows a straightforward generalization to treat ac voltages applied to the ring. The technical calculations are presented in the Appendix.

III. MODEL

The 2D quantum dot (see the left panel in Fig. 2) is biased with several voltages $\{V_i\}$ at M ballistic quantum point contacts (QPCs) with $N_i, i=1,\ldots,M$ orbital channels. The reservoirs can be capacitively coupled to the dot via capacitances C_i. An additional set of voltages $\{V_{gi}\}$ is applied to (several) gates with capacitances C_{gi}. All perturbations are assumed to be at the same frequency ω, which is not necessarily small (adiabatic).

The dot is in the universal regime,[36] when the Thouless energy $E_{\mathrm{Th}}=\hbar/\tau_{\mathrm{erg}}$ is large. The dots with area $A=\pi L^2$ (taken circular) are either diffusive with mean free path $l\ll L$, or ballistic, with $l\gg L$ and chaotic classical dynamics (in the latter case the substitution $l\to\pi L/4$ should be used). The mean level spacing (per spin direction) $\Delta=2\pi\hbar^2/(m^*A)$ and the total number of ballistic channels N together define the dwell time $\tau_d=h/(N\Delta)\gg\tau_{\mathrm{erg}}$. We also require that $eV\ll N\Delta$ when we can treat the nonlinearity only to $(eV)^2$. Scattering is spin-independent and this spin degeneracy is accounted for by the coefficient ν_s.

The noninteracting electrons are treated using the scattering matrix approach and random matrix theory (RMT) for the energy-dependent scattering matrix $\mathcal{S}(\varepsilon)$. For details we refer the reader to reviews.[36,37] In this approach the fundamental property of a dot is its scattering matrix $\mathcal{S}$ distributed over circular ensembles of proper symmetry; see Ref. 36. (An alternative method is the Hamiltonian approach based on the properties of the dot's Hamiltonian $\mathcal{H}$ taken from a Gaussian ensemble.[37]) Transport properties of chaotic dots in RMT for matrices $\mathcal{S}$ or $\mathcal{H}$ are usually expressed in terms of an effective, magnetic-field-dependent number of channels. Predictions based on this approach are in good agreement with experiment. For multichannel samples with $N\gg 1$ we use the diagrammatic technique described in Refs. 38 and 39.

However, when interactions are present, this treatment should be modified. The approach, which assumes that in a pointlike scatterer the interactions appear in the form of a self-consistent potential, was introduced by Büttiker and co-authors[40] on the basis of gauge invariance and charge conservation. This (Hartree) approach neglects contributions leading to Coulomb blockade (Fock terms), but is a good approximation for open systems. If the screening in the dot inside the medium with dielectric constant ε is strong, $r_s=(k_Fa_B)^{-1}=e^2/(\varepsilon\hbar v_F)\lesssim 1$, an RPA treatment of Coulomb interactions is sufficient. For large dots, $L\gg a_B$, the details of screening potential on the scale $\sim a_B$ are not important and we can assign an electric potential $U(\vec{r},t)$ defined by excess electrons at $\vec{r},t$ at any point $\vec{r}$ of the sample. If, additionally, the number of ballistic channels N is much smaller than the dimensionless conductance of a closed sample, $g_{\mathrm{dot}}=E_{\mathrm{Th}}/\Delta\gg N$, the potential drops over the contacts and therefore in the interior of the dot it can be taken uniformly ("zero-mode approximation").[37] This potential shifts the bottom of the energy band in the dot and thus modifies the $\mathcal{S}$-matrix. As a consequence, electrons with kinetic energy E have an electrochemical potential $\tilde{E}_\alpha=E-eV_\alpha$ in the contact α and $\tilde{E}=E-eU$ in the dot. (We point out that we neglect the quantum pumping in the dot and consequently the $\mathcal{S}$-matrix depends only on one energy.) Recently, Brouwer, Lamacraft, and Flensberg demonstrated that this self-consistent approach gives the leading order in an expansion in the inverse number of channels $1/N\ll 1$.[41] Therefore, our analytical results present the leading order effect, valid for $1/N\ll 1$.

In the self-consistent approach the influx of charge changes the internal electrical potential of the dot $U(t)$, which in turn affects the currents incoming through each conducting lead and/or redistributes charges among the nearby conductors (gates). Such capacitive coupling can often be estimated simply from the geometrical configuration. For example, the capacitance of a dot covered by a top gate at short distance $d\ll L$ is $C\sim\varepsilon L^2/d$ and a single quantum dot has $C\sim\varepsilon L$. The ratio of charging energy $E_c\sim e^2/C$ to mean level spacing Δ characterizes the interaction strength. It is proportional to the ratio of the smallest geometrical scale to the effective Bohr's radius, $E_c/\Delta\sim\min\{d,L\}/a_B$. We refer to interactions as strong if $E_c\gg\Delta$ and weak if $E_c\ll\Delta$.

IV. IMPORTANCE OF BIAS MODE

We suppose for simplicity that at equilibrium the voltages $V_1=V_2=V_0$ are set. In the following we consider the situation

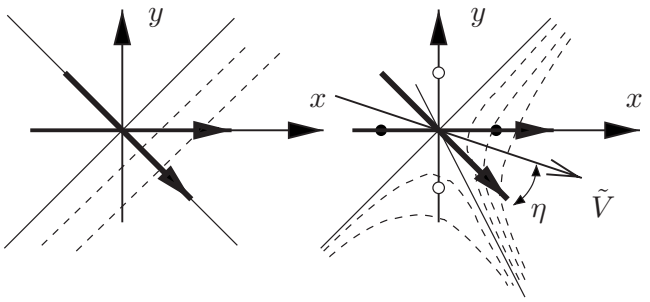

FIG. 3. Depending on the bias mode, the experiment probes different transport properties. Plots present (left) linear and (right) nonlinear components of the current as functions of $x=V_1-V_0$ and $y=V_2-V_0$; the dashed curves correspond to equal currents. Thin line shows fixed V_2 and $I(\tilde{V})$ is a function of source voltage $\tilde{V}=V_1$. Thick line corresponds to fixed V_1+V_2, such that $I(\tilde{V})$ depends only on $\tilde{V}=(V_1-V_2)/\sqrt{2}$. Full and empty dots on the right figure correspond to the forward or reverse configurations shown in Fig. 1.

when the (single) gate voltage V_0 is held fixed at its equilibrium value. Experiments can be performed in different *bias modes*, usually either (i) with fixed drain voltage V_2 or (ii) at fixed V_1+V_2 (the variations of the voltages at the contacts are equal in magnitude but opposite in sign). These different modes correspond to straight lines in the $\{V_1,V_2\}$ plane shown in Fig. 3.

Let us consider the nonlinear current as a function $I(x,y)$, where $x=V_1-V_0$ and $y=V_2-V_0$ are deviations of contact voltages from equilibrium. For generality, we consider below a situation when the linear combination $-x\sin(\eta-\pi/4)+y\cos(\eta-\pi/4)=0$ is held fixed and the only variable is

$$\tilde{V}=x\cos(\eta-\pi/4)+y\sin(\eta-\pi/4). \tag{3}$$

This corresponds to a rotation of the original x,y axes such that the new coordinate axis $\tilde{V}$ makes an angle η with the $y=-x$ line, as illustrated in Fig. 3. The value of η fully characterizes the bias mode. Now the two modes introduced above are simply (i) $\eta=\pi/4$, which implies $\tilde{V}=x$, and (ii) $\eta=0$, which implies $\tilde{V}=(x-y)/\sqrt{2}$ and corresponds to an asymmetric variation of the voltages.

The linear current depends only on $x-y$ (dashed lines on the left panel in Fig. 3 correspond to the lines of equal currents) and in any bias mode the measured linear current I_{lin} is the same for a given $x-y$. If we consider the nonlinear current I as a function of x,y, it is by construction a bilinear function of x,y. As in the linear case the current must vanish if the voltages are the same and thus $I=0$ for $x-y=0$. Therefore, the bilinear function must be of the form

$$I=I_0[(x+y)\cos\phi+(x-y)\sin\phi](x-y) \tag{4}$$

with unknown (generally fluctuating) parameters I_0 and $\phi\in(-\pi/2,\pi/2]$. It is important that the qualitative behavior of $I(x,y)$ depends on the interaction strength: One could expect that transport depends not only on voltages in the leads, but also on the internal nonequilibrium potential U of the sample. This potential can be found if potentials in all reservoirs and the nearby gate are known.

In the limit of weak interactions the equilibrium point V_0 is important, and if we reverse the bias voltage, $(V,0)\to(0,V)$ the current is fully reversed; that is $\partial_{xx}^2 I=-\partial_{yy}^2 I$. For the current defined in Eq. (4) it is possible only when $I\propto(x-y)(x+y)\Rightarrow\phi=0$. Another way to see this is to use the usual expression for the total current in terms of scattering matrices. In this formula the current depends on the difference between Fermi distributions in the leads $\propto f(\varepsilon-ex)-f(\varepsilon-ey)$, and its expansion up to the second order yields $f''(\varepsilon)\times(x^2-y^2)$. The lines of equal current are curved and directions $\eta=0,\pm\pi/2$ correspond to zero current directions. Thus the dependence of current on the angle η is strong. In addition this approach predicts that the current through a two-terminal sample is symmetric with respect to the magnetic flux inversion.

In contrast, for strong interactions, the value of V_0 is irrelevant and the nonequilibrium electrical potential U is independent of V_0. In this case current depends only on the voltage difference $x-y$ and thus $I\propto(x-y)^2\Rightarrow|\phi|=\pi/2$. The equal-current lines are straight and the picture is similar to the left plot in Fig. 3 for linear transport. Therefore, we do not expect any nontrivial dependence of the nonlinear current on the choice of the bias mode.

It is noteworthy that qualitative considerations can predict neither the sign nor the magnitude of I_0. The only general conclusion which we can make for a weakly or strongly interacting dot is $I(x,y)\propto x^2-y^2$ and $I(x,y)\propto(x-y)^2$, respectively. Experiments extract derivatives of I with respect to the applied voltages. Importantly, this derivative depends on the chosen direction η. The nonlinear current measured in this bias mode is

$$I(\eta)=I_0\tilde{V}^2\cos\eta\sin(\phi+\eta). \tag{5}$$

The current is zero when $\eta=-\phi$ and $\eta=\pm\pi/2$, and the bisectrix of the angle between the two zero-current directions at $\eta=-\phi/2+(\pi/4)\mathrm{sgn}\,\phi$ maximizes $\partial^2 I/\partial\tilde{V}^2$.

Sometimes experiments extract information on nonlinearity from measurements in different connections schematically shown in the central and right panels in Fig. 2: "Forward" connection corresponds to $x=\pm V, y=0$, while "reverse" connection for the same voltage configuration corresponds to $x=0, y=\pm V$. The gate voltages V_g are kept fixed. In Fig. 3 these forward and reverse points are indicated by black and white dots respectively. To find the nonlinear conductance Marlow *et al.*[8] and Löfgren *et al.*[19] determine the difference of conductance at these measurement points. Löfgren *et al.*[19,42] use the term "rigidity" for samples for which $G_f(V)=G_r(-V)$ in the points $f^+=(V,0)$ and $r^-=(0,-V)$.[42] Equation (4) gives the nonlinear contribution $\mathcal{G}$ to the full conductance $G_{f,r}(\pm V)$:

$$\mathcal{G}\propto I_0[(x-y)\sin\phi+(x+y)\cos\phi]. \tag{6}$$

Thus for a sample which is called rigid this implies $I_0\cos\phi\to 0$. Since $I_0=0$ would mean that there is no second-order response, we must have $\cos\phi\to 0$ which is the case for samples with strong interaction. In other words, "rigidity" in

samples which exhibit $O(V^2)$ current is equivalent to strong Coulomb interactions.

On the other hand, comparison of data at another pair of points $f^+=(V,0)$ and $r^+=(0,V)$ gives $G_f(V)-G_r(V) \propto I_0 \sin\phi$ and provides *additional* information about the two fluctuating quantities I_0, ϕ. Reference 19 expects that a left-right (LR) symmetric system has $G_f(V)=G_r(V)$. Therefore rigid and LR-symmetric sample should necessarily have $I_0 \to 0$ and thus could not exhibit a second-order current $O(V^2)$. This point is discussed more quantitatively in Sec. V A.

It is important to note that to find the linear dc current one needs to know only $x-y=V_1-V_2$, while for the nonlinear current, in general, one needs two variables $x=V_1-V_0$, $y=V_2-V_0$ or any independent pair of their linear combinations. The projection of the vector (V_1,V_2,V_0) on the $V_1+V_2+V_0$=const plane uniquely defines the nonlinear current. This projection can be parametrized by the pair of Cartesian (x,y) or axial coordinates $(\tilde{V},\eta)$. However, if in the experiment the voltages $V_{1,2}$ were fixed, this would not be enough to define (x,y) uniquely. In this case Ref. 19 points to the importance of the reference point V_0. Indeed, one could arrive at the point with a given (V_1,V_2) from any equilibrium point and the measured current would depend on V_0. We prefer to characterize the measurement by the pair $(\tilde{V},\eta)$ instead of three variables (V_1,V_2,V_0) because of the simplicity of the final results. The weaker the interaction (or the stronger the capacitive coupling of the sample to the nearby gate) the more important the role of η chosen in experiment.

We illustrate this important conclusion by quantitative results for nonlinear conductance $\mathcal{G} \propto \partial^2 I/\partial \tilde{V}^2$ in the following sections. We point out that conductance with respect to the voltage difference $V=V_1-V_2$ is often used, even when a linear combination $\tilde{V}$ is actually varied in experiment. Voltages $\tilde{V}$ and V are related, $\tilde{V}=V/\sqrt{2}\cos\eta$, and one can straightforwardly find $\partial^2 I/\partial V^2$.

V. GENERATION OF dc IN QUANTUM DOTS

Now we quantify the qualitative arguments of Sec. IV and consider the more general situation of a dc current generated by an ac bias. If at first we neglect Coulomb interactions, the nonlinear dc current I_α in response to the Fourier components $V_{\beta,\omega}=V_\beta e^{i\phi_\beta}$ of the ac voltages applied at the contacts $\beta=1,\ldots,M$, can be expressed with the help of the dc-conductance matrix $g_{\alpha\beta}(\varepsilon)$ of the dot at the energy ε[28]

$$I_\alpha = \frac{\nu_s e^3}{h}\int d\varepsilon \frac{f(\varepsilon+\hbar\omega)+f(\varepsilon-\hbar\omega)-2f(\varepsilon)}{(\hbar\omega)^2} \times \sum_{\beta=1}^{M} g_{\alpha\beta}(\varepsilon)|V_{\beta,\omega}|^2, \tag{7}$$

$$g_{\alpha\beta}(\varepsilon) = \mathrm{tr}[\mathbb{1}_\alpha \delta_{\alpha\beta} - \mathcal{S}^\dagger(\varepsilon)\mathbb{1}_\alpha \mathcal{S}(\varepsilon)\mathbb{1}_\beta]. \tag{8}$$

If we now include interactions using a self-consistent potential U_ω this formula is modified:[28] In Eq. (7) the Fourier components of the voltages at *all* contacts are shifted down by the Fourier component of the internal potential $-U_\omega$

$$U_\omega = \sum_\gamma u_\gamma V_{\gamma,\omega}, \quad u_\gamma = \frac{\sum_\beta G_{\beta\gamma}(\omega) - i\omega C_\gamma}{\sum_{\beta\gamma} G_{\beta\gamma}(\omega) - i\omega C_\Sigma}, \tag{9}$$

$$G_{\beta\gamma}(\omega) = \frac{\nu_s e^2}{h}\int d\varepsilon\, \mathrm{tr}[\mathbb{1}_\beta\mathbb{1}_\gamma - \mathbb{1}_\gamma \mathcal{S}^\dagger(\varepsilon)\mathbb{1}_\beta \mathcal{S}(\varepsilon+\hbar\omega)] \times \frac{f(\varepsilon)-f(\varepsilon+\hbar\omega)}{\hbar\omega}. \tag{10}$$

In Eq. (9) the index γ runs not only over real leads $1,\ldots,M$, but also over all gates gi. However, when $\gamma \in \{gi\}$ the ac conductance $G_{\beta\gamma}(\omega)$ is absent and only capacitive coupling $i\omega C_\gamma$ remains in the numerator. We point out that the matrix $G(\omega)$ of dynamical ac conductance at frequency ω given in Eq. (10) should not be confused with the degenerate matrix $g(\varepsilon)$ of energy-dependent dc conductances of electrons with kinetic energy ε given in Eq. (8).

The results of Ref. 28 can be expressed in terms of the dc conductances $g_{\alpha\beta}$ and frequency-dependent characteristic potentials u_γ,

$$I_\alpha = \frac{\nu_s e^3}{h}\int d\varepsilon \frac{f(\varepsilon+\hbar\omega)+f(\varepsilon-\hbar\omega)-2f(\varepsilon)}{(\hbar\omega)^2} \times \sum_{\beta\gamma} g_{\alpha\beta}(\varepsilon)\mathrm{Re}\, u_\gamma |V_{\beta,\omega}-V_{\gamma,\omega}|^2. \tag{11}$$

Here Re u_γ stands for the real part of u_γ, which is generally a complex quantity. In contrast to Eq. (7), Eq. (11) is expressed via differences of voltages applied to all present conductors. Therefore, the current is gauge-invariant. The charge conservation, $\Sigma_\alpha I_\alpha=0$, is obvious from Eq. (8).

From this point on we consider Eq. (11), a specific expression of Eq. (1), in detail for several regimes. In Sec. V A we discuss the nonlinear current due to dc applied voltages (previously considered in Ref. 43) and the importance of different bias modes in experiments in two-terminal quantum dots. In Sec. V B we consider the frequency dependence of $\mathcal{G}_s(\omega)$ and $\mathcal{G}_a(\omega)$.

A. Nonlinearity in quantum dots

In the static limit[43] $\hbar\omega/T \to 0$ the integrand in the first line of Eq. (11) simplifies to $f''(\varepsilon)$ and for $\hbar\omega/N\Delta \to 0$ the derivatives u_γ are real and expressed via subtraces of the Hermitian Wigner-Smith matrix $\mathcal{S}^\dagger\partial_\varepsilon\mathcal{S}/(2\pi i)$[44,45]

$$I_\alpha = \frac{-\nu_s e^3}{h}\sum_{\beta\gamma}\int f'(\varepsilon)d\varepsilon g'_{\alpha\beta}(\varepsilon)u_\gamma(V_\beta - V_\gamma)^2, \tag{12}$$

$$u_\gamma = \frac{C_\gamma/\nu_s e^2 - \int d\varepsilon f'(\varepsilon)\mathrm{tr}\,\mathbb{1}_\gamma \mathcal{S}^\dagger\partial_\varepsilon\mathcal{S}/(2\pi i)}{C_\Sigma/\nu_s e^2 - \int d\varepsilon f'(\varepsilon)\mathrm{tr}\,\mathcal{S}^\dagger\partial_\varepsilon\mathcal{S}/(2\pi i)}. \tag{13}$$

For a two-terminal sample the nonlinear current through the first lead is

$$I_1 = \frac{-\nu_s e^3}{h}\int f'(\varepsilon) g_{11}'(\varepsilon) d\varepsilon \times\left[\sum_i u_{gi}[(V_1 - V_{gi})^2 - (V_2 - V_{gi})^2] + (u_2 - u_1)(V_1 - V_2)^2\right]. \quad (14)$$

The characteristic potentials in the last term of Eq. (14) are sensitive to the asymmetry of the contacts. Indeed, in a strongly interacting dot $u_{gi}=0$ and $u_2-u_1\approx(N_2-N_1)/N$. The current magnitude grows with asymmetry due to the last term in Eq. (14). On the other hand, the sign of I_1 is random because of quantum fluctuations of g_{11}' around zero.[46] As a consequence, if in an experiment the Fermi level is shifted by $\delta\mu_F \sim N\Delta/2\pi$ (or the shape of the dot is changed) the sign of nonlinearity can be inverted.

Different modes of bias having been discussed in Sec. IV, we concentrate here on the (anti)symmetric conductances through the quantum dot at fixed gate voltages. When the reservoir voltages are varied in the η direction, the nonlinear current is given by the expression

$$I = \frac{-2\nu_s e^3}{h}\int f'(\varepsilon) g_{11}'(\varepsilon) d\varepsilon[(1-u_1-u_2)\sin\eta + (u_2-u_1)\cos\eta]\cos\eta \widetilde{V}^2, \quad (15)$$

and one can define exactly the unknown parameters I_0, ϕ which we introduced in the qualitative argument leading to Eq. (5). Depending on η one measures different linear combinations of conductances. If we consider conductances $\partial^2 I/2\partial\widetilde{V}^2$ in units of $\nu_s e^3/h$, Eqs. (2) and (15) yield

$$\mathcal{G}_{a,s} = \frac{2\pi\cos^2\eta\int d\varepsilon\, d\tilde{\varepsilon} f'(\varepsilon) f'(\tilde{\varepsilon}) \chi_1(\varepsilon)\chi_{2,a(s)}(\tilde{\varepsilon})}{\Delta^2\left[C_\Sigma/(e^2\nu_s) - \int d\varepsilon f'(\varepsilon)\mathrm{tr}\, \mathcal{S}^\dagger\partial_\varepsilon\mathcal{S}/(2\pi i)\right]} \quad (16)$$

expressed in terms of fluctuating functions χ and a traceless matrix $\Lambda=(N_2/N)\mathbb{1}_1-(N_1/N)\mathbb{1}_2$:

$$\chi_1(\varepsilon) = (\Delta/2\pi)\partial_\varepsilon\, \mathrm{tr}\, \Lambda\mathcal{S}^\dagger\Lambda\mathcal{S}, \quad (17)$$

$$\chi_{2,a}(\varepsilon) = (i\Delta/2\pi)\mathrm{tr}\, \Lambda[\mathcal{S}^\dagger, \partial_\varepsilon\mathcal{S}], \quad (18)$$

$$\chi_{2,s}(\varepsilon) = \Delta\left(\frac{C_0\tan\eta + C_2 - C_1}{e^2\nu_s} + \frac{N_2-N_1}{N}\frac{\mathrm{tr}\, \mathcal{S}^\dagger\partial_\varepsilon\mathcal{S}}{2\pi i} + \frac{1}{2\pi i}\mathrm{tr}\, \Lambda\{\mathcal{S}^\dagger, \partial_\varepsilon\mathcal{S}\}\right). \quad (19)$$

Standard calculations using the Wigner-Smith and/or $\mathcal{S}$-matrix averaging[38,39,47] yield $\langle\mathcal{G}_a\rangle=\langle\mathcal{G}_s\rangle=0$. This result signifies that the nonlinear current through a quantum dot is indeed a quantum effect. As a consequence the size of the measured nonlinearity must be evaluated from correlations of $\mathcal{G}_a, \mathcal{G}_s$.

The functions $\chi_1(\varepsilon,\Phi)$ and $\chi_{2,a/s}(\varepsilon',\Phi')$ are uncorrelated, and their autocorrelations[16] readily allow one to find statistical properties of $\mathcal{G}_{a,s}$. Our results can be expressed in terms of diffuson $\mathcal{D}$ or Cooperon $\mathcal{C}$ in a time representation, $\exp(-\tau/\tau_\mathcal{D})$ and $\exp(-\tau/\tau_\mathcal{C})$. Both can be introduced using the $\mathcal{S}$-matrix correlators[48] (correlations of retarded and advanced Green functions lead to the same expression up to a normalization constant[37]). We have

$$\mathcal{S}(\tau,\Phi) = \int\frac{d\varepsilon}{2\pi\hbar}\mathcal{S}(\varepsilon,\Phi)e^{i\varepsilon\tau/\hbar},$$

$$\langle\mathcal{S}_{ij}(\tau,\Phi)\mathcal{S}_{kl}^*(\tau',\Phi')\rangle = (e^{-\pi/\tau_\mathcal{D}}\delta_{ik}\delta_{jl} + e^{-\pi/\tau_\mathcal{C}}\delta_{il}\delta_{jk}) \times\frac{\Delta}{2\pi\hbar}\delta(\tau-\tau')\theta(\tau), \quad (20)$$

$$\tau_{\mathcal{C},\mathcal{D}} = \frac{h}{N_{\mathcal{C},\mathcal{D}}\Delta}, \quad \begin{Bmatrix} N_\mathcal{C} \\ N_\mathcal{D}\end{Bmatrix} = N + \frac{(\Phi\pm\Phi')^2}{4\Phi_0^2}\frac{hv_F l}{L^2\Delta}. \quad (21)$$

We also introduce the electrochemical capacitance C_μ[49] which relates the nonquantized mesoscopically averaged excess charge $\langle Q\rangle$ in the dot in response to small shift of the voltages δV at all gates. In addition the charge relaxation time τ_{RC} of the dot is conveniently introduced by this electrochemical capacitance and the total contact resistance,

$$C_\mu = \frac{\langle\delta Q\rangle}{\delta V} = \frac{C_\Sigma}{1 + C_\Sigma\Delta/(\nu_s e^2)}, \quad \tau_{\mathrm{RC}} = \frac{hC_\mu}{\nu_s N e^2}. \quad (22)$$

The denominator of Eq. (16) is a self-averaging quantity, $\langle(\cdots)^2\rangle=\langle(\cdots)\rangle^2=\Delta^2(C_\Sigma/C_\mu)^2$. Using the diffusons and Cooperons defined in Eq. (20) we find the following correlations of $\mathcal{G}_a$ and $\mathcal{G}_s$:

$$\begin{Bmatrix}\langle\mathcal{G}_a(\Phi)\mathcal{G}_a(\Phi')\rangle \\ \langle\mathcal{G}_s(\Phi)\mathcal{G}_s(\Phi')\rangle\end{Bmatrix} = \begin{Bmatrix}\mathcal{F}_\mathcal{D} - \mathcal{F}_\mathcal{C} \\ \mathcal{F}_\mathcal{D} + \mathcal{F}_\mathcal{C} + X\end{Bmatrix}(\mathcal{F}_\mathcal{D} + \mathcal{F}_\mathcal{C}) \times\left(2\cos^2\eta\frac{2\pi}{\Delta}\frac{C_\mu}{C_\Sigma}\right)^2\frac{N_1^3N_2^3}{N^6}, \quad (23)$$

$$\mathcal{F}_\lambda = \left(\frac{\Delta T}{2\hbar^2}\right)^2\int\frac{\tau_\lambda\tau^2 e^{-\pi/\tau_\lambda}}{\sinh^2\pi T\tau/\hbar}d\tau, \quad (24)$$

$$X = \frac{N^2}{2N_1N_2}\left(\frac{C_0\tan\eta + C_2 - C_1}{\nu_s e^2/\Delta} + \frac{N_2-N_1}{N}\right)^2. \quad (25)$$

There are two very different contributions to Eq. (23), $\mathcal{F}_{\mathcal{C},\mathcal{D}}$ due to quantum interference and X defined by the classical response of the internal potential to external voltage. The terms denoted by $\mathcal{F}_{\mathcal{C},\mathcal{D}}$ are sensitive to temperature, magnetic field, and decoherence. Asymptotical values of $\mathcal{F}$ in the low temperature, $T\ll\hbar/\tau_\lambda$, or high temperature limits, $T\gg\hbar/\tau_\lambda$, are $\mathcal{F}_\lambda\to 1/N_\lambda^2=(\tau_\lambda\Delta/h)^2$ and $\mathcal{F}_\lambda\to\Delta/(12TN_\lambda) = \tau_\lambda\Delta^2/(12hT)$, respectively.

The term denoted by X and given by Eq. (25) contains only quantities specifying the geometry of the sample and gates and the bias mode. In a real experiment the coupling due to capacitances $C_{1,2}$ is usually stronger then that of the

external gates, $C_{1,2} \gg C_0$. Symmetrization of the circuit $C_1 = C_2$ can diminish the value of X. If in addition $N_1 = N_2$ and $\eta = 0$ (used in the experiments,[9,10]) we have $X \to 0$. Thus such a symmetric setup and bias mode minimize the fluctuations of the nonlinear current and actually would be best for an accurate measurement of *linear* transport. Indeed, this regime is not affected by the fluctuations of capacitive coupling u_0 of the dot with the nearby gate and thus minimizes fluctuations of $\mathcal{G}_s$ around 0.

Fluctuations of $\mathcal{G}_a, \mathcal{G}_s$ are given by different expressions, see the first line of Eq. (23), where the first term is due to $\langle \chi_{2,a}^2 \rangle$ or $\langle \chi_{2,s}^2 \rangle$. Importantly, $\langle \chi_{2,s}^2 \rangle$ contains both quantum $\mathcal{F}_\lambda \lesssim 1/N_\lambda^2$ and classical X contributions. If the classical term dominates, $X \gg 1/N^2$, the current is mostly symmetric, $\mathcal{G}_s^2 \gg \mathcal{G}_a^2$. This could be expected either for a weakly interacting dot or a very asymmetric setup, $N_1 \neq N_2$.[16] However, if the classical term is reduced due to, e.g., the bias mode, the fluctuations of $\mathcal{G}_a$ and $\mathcal{G}_s$ become comparable. This experimentally important conclusion remains valid for *any interaction strength*. (Particularly, it leads to a very wide distribution of the Aharonov-Bohm phase considered in Sec. VI.)

Experiments of Zumbühl *et al.*[10] and Leturcq *et al.*[9] are performed in this regime when $\eta = 0$ and $X \to 0$. Data in Ref. 10 demonstrate that the part of the total current symmetrized with respect to magnetic field is by far dominated by linear conductance. From Eq. (23) we expect mesoscopic fluctuations in linear conductance to be $\sim N^2$ times larger then those of $\mathcal{G}_s \Delta$. Thus, only when the number of channels is decreased will the nonlinear $\mathcal{G}_s$ become noticeable. A clear observation of $\mathcal{G}_s$ without linear transport contribution was performed in a dc Aharonov-Bohm experiment by Angers *et al.*[11] in the mode $\eta = \pm \pi/4$ (only one contact voltage was varied). This allowed us to evaluate the interaction strength from the ratio of $\mathcal{G}_s/\mathcal{G}_a$.

Experiments of Marlow *et al.*[8] and Löfgren *et al.*[19] measure the full two-terminal conductance and extract nonlinear conductance properties related to various spatial symmetries of the dot. Although the current through a weakly interacting sample is field-symmetric, this is not true in general. Samples of Ref. 19 differ in "rigidity" and degree of symmetry. Rigid samples, $u_0 \to 0$, with left-right (LR) and up-down (UD) symmetry should have $(u_2 - u_1)_s = 0$ and $(u_2 - u_1)_a = 0$, respectively, according to the expectations of Löfgren *et al.*[19] (indices s and a mean the symmetric and antisymmetric part in magnetic field).

Due to quantum fluctuations, in experiment none of these symmetry relations can be exactly fulfilled; see Eq. (23). According to Eq. (15), the difference in the full conductances $g = (h/\nu_s e^2) I/V$ measured between different points probes different characteristic potentials. Reference 19 defines three differences $g_{\mathrm{i,ii,iii}}$ for three pairs of points in the forward and reverse connection discussed after Eq. (5). Using Eq. (23) we find (i) $g_{\mathrm{i}} \equiv g_f(V,B) - g_r(-V,B) \propto u_0$, (ii) $g_{\mathrm{ii}} \equiv g_f(V,B) - g_f(V,-B) \propto (u_2 - u_1)_a$, and (iii) $g_{\mathrm{iii}} \equiv g_f(V,B) - g_f(-V,-B) \propto (u_0 + u_2 - u_1)_s$. The ensemble average of these differences vanishes and their fluctuations for $C_{1,2} = 0, N_1 = N_2$ are given by

$$\begin{Bmatrix} g_{\mathrm{i}}^2 \\ g_{\mathrm{ii}}^2 \\ g_{\mathrm{iii}}^2 \end{Bmatrix} = \begin{Bmatrix} X \\ \mathcal{F}_\mathcal{D} - \mathcal{F}_\mathcal{C} \\ X + \mathcal{F}_\mathcal{D} + \mathcal{F}_\mathcal{C} \end{Bmatrix} (\mathcal{F}_\mathcal{D} + \mathcal{F}_\mathcal{C}) \left(\frac{\pi e V}{2\Delta} \frac{C_\mu}{C} \right)^2,$$

where $X = 2(C/C_\mu - 1)^2$ is found from Eq. (25) at $\eta = \pm \pi/4$. In weakly interacting dots $C_\mu/C \to 0$ and only magnetic-field symmetric signals g_{i} and g_{iii} survive. In strongly interacting ("rigid") dots $C_\mu/C \to 1$ and g_{ii} becomes similar to g_{iii}. We point out that even if the rigid samples are made symmetric with respect to left-right inversion, the quantum fluctuations of the sample properties are unavoidable and $g_{\mathrm{ii}}^2 \neq 0$ at $\Phi \neq 0$. For high magnetic fields and arbitrary interactions $\mathcal{F}_\mathcal{C} \to 0$ and experiment should observe $g_{\mathrm{i}}^2 + g_{\mathrm{ii}}^2 = g_{\mathrm{iii}}^2$. Clearly fluctuations exist also for large magnetic fields beyond the range of applicability of RMT. Experimental data (see inset of the Fig. 6 in Ref. 19) show that $g_{\mathrm{i}}^2 + g_{\mathrm{ii}}^2 \sim g_{\mathrm{iii}}^2$. It is hard to make a quantitative comparison with Refs. 8 and 19, since the quantum fluctuations in the nonlinear conductance exist possibly on the background of classical effects due to macroscopic symmetries. We expect that quantum effects become more pronounced as contacts are narrowed.

To conclude this subsection we briefly discuss here the case of a macroscopically asymmetric setup. If the experiment were aimed at measuring large $\mathcal{G}_a$ compared to $\mathcal{G}_s$, one would try to minimize $\mathcal{G}_s$ by adjusting the setup. Such a procedure minimizes the value of X in Eq. (25). For $C_{1,2} = 0$, $\eta = \pi/4$ the role of asymmetric contacts $N_1 \neq N_2$ was discussed in Ref. 16. Analogously, one could consider a more general case of $C_{1,2}$ and an arbitrary bias mode η. This is especially important if the difference $C_1 \neq C_2$ cannot be neglected due to occasional loss of contact symmetry.

The results of an experiment could also be affected by the presence of classical resistance loads $r_{1,2}$ between macroscopic reservoirs and the dot (shown in Fig. 2). Swapping of such resistances in the experiment, when connection is switched between "forward" and "reverse"[19] affects the voltage division between loads. If we assume the capacitive connection of the dot and reservoirs is still the same, the modification of the expression for u_γ in Eq. (9) is straightforward, $\Sigma_\beta G_{\beta\gamma} \to \Sigma_\beta G_{\beta\gamma}/(1 + r_\gamma \Sigma_\beta G_{\beta\gamma})$. Naturally, at large r_γ, $(2e^2 N_\gamma/h) r_\gamma \gg 1$, the main drop of the voltage occurs over the resistor r_γ and not over the QPCs. As a consequence, if $r_{1,2} \neq 0$, values of $u_{1,2}$ can become unequal due to $r_1 \neq r_2$ and this leads to the classical circuit asymmetry which we do not consider here.

B. Rectification in quantum dots

Here we consider the dc generated by a quantum dot subject to an ac bias at the frequency ω. In experiment at high bias frequency $\omega \tau_d \gtrsim 1$ current is usually measured at zero frequency. In contrast, at small bias frequency $\omega \tau_d \ll 1$ higher harmonics (for instance the second harmonic 2ω) can be measured. However, up to corrections small due to $\omega \tau_d \ll 1$, the second harmonic is just equal to the rectified current, $I_{2\omega} \approx I_0$. Therefore, to leading order, our results for the rectified current describe both experiments.

Generally, there are several important time scales characteristic for time-dependent problems in chaotic quantum

dots. To see how they appear let us first consider frequency-dependent linear transport of noninteracting electrons. Its statistics usually depend only on the flux-dependent time scales $\tau_{\mathcal{C},\mathcal{D}}$; see Eq. (21). If we consider an analog of UCF $\langle G^2(\Phi)\rangle$ for the frequency-dependent conductances introduced in Eq. (10), we find

$$\langle G(\omega,\Phi)G(\omega',\Phi')\rangle = \left(\frac{\nu_s e^2}{h}\frac{N_1N_2}{N}\right)^2 \sum_{\lambda=\mathcal{C},\mathcal{D}} \left(\frac{\Delta T}{2\hbar^2}\right)^2 \int \frac{\tau_\lambda d\tau}{\omega\omega'} \times \frac{e^{-\pi/\tau_\lambda}(e^{i\omega\tau}-1)(1-e^{i\omega'\tau})}{[1-i(\omega+\omega')\tau_\lambda/2]\sinh^2\pi T\tau/\hbar}. \tag{26}$$

The presence of $i\omega\tau_\lambda$ in the diffuson and Cooperon contributions in the second line of Eq. (26) is due to the energy dependence of the scattering matrix $\mathcal{S}(\varepsilon)$, which usually brings up imaginary corrections to the matrix-element correlators.

In a dc problem $\omega\to 0$ it is usually useful to introduce a dimensionless number of channels $N_{\mathcal{C},\mathcal{D}}$ modified by the magnetic field; see Eq. (21). In this limit at $T\to 0$ the integration in Eq. (26) becomes straightforward, and summation is then performed over N_λ^{-2}. For equal magnetic fields, $\Phi=\Phi'$, we have $N_\mathcal{D}=N$, but $N_\mathcal{C}$ is strongly modified by large fields, $N_\mathcal{C}\to\infty$, which suppresses the weak localization correction and diminishes UCF. However, for an ac problem (especially for $\omega\tau_d\gtrsim 1$) it is more convenient to express results in terms of dimensionless quantities $\omega\tau_\mathcal{C},\omega\tau_\mathcal{D}$. For example, from Eq. (26) the statistics of conductance can be easily evaluated: $\langle|G(\omega,\Phi)|^2\rangle/\langle G(0,\Phi)^2\rangle\sim 1/(\omega\tau_d)$ and the real and imaginary parts of conductance are similar and uncorrelated at high frequency $\omega\tau_d\gg 1$.

Inclusion of interactions introduces an (additional) dependence on τ_{RC}, the charge-relaxation time defined in Eq. (22). To leading order in $1/N\ll 1$ the effect of interactions is often to substitute $\tau_d\to\tau_{\mathrm{RC}}$ in the noninteracting results, e.g., for the linear conductance[49] or shot noise.[45,50] Interestingly, the subleading corrections depend on both τ_{RC} and τ_d, e.g., in the weak localization correction in the absence of magnetic field.[49] When the magnetic field is increased to values which finally break time-reversal symmetry, the appearance of different time scales $\tau_{\mathcal{C},\mathcal{D}}$ is expected; see, e.g., Eq. (26). Therefore at intermediate magnetic fields, when $\tau_\mathcal{D}\neq\tau_\mathcal{C}$, and the interactions taken into account, $\tau_{\mathrm{RC}}\neq\tau_d$, the solution of an ac problem is expected to show a complicated dependence on all these time scales.

Indeed, if we consider the rectified current such an interplay between $\tau_{\mathcal{C},\mathcal{D}}$ and τ_{RC} does appear. We find $\langle\mathcal{G}_a\rangle=\langle\mathcal{G}_s\rangle=0$ and present below results for correlations of $\mathcal{G}_a$ and $\mathcal{G}_s$:

$$\begin{Bmatrix}\langle\mathcal{G}_a(\Phi)\mathcal{G}_a(\Phi')\rangle\\ \langle\mathcal{G}_s(\Phi)\mathcal{G}_s(\Phi')\rangle\end{Bmatrix} = \begin{Bmatrix}\mathcal{F}_{U,\mathcal{D}}(\omega)-\mathcal{F}_{U,\mathcal{C}}(\omega)\\ \mathcal{F}_{U,\mathcal{D}}(\omega)+\mathcal{F}_{U,\mathcal{C}}(\omega)+X(\omega)\end{Bmatrix} \times[\mathcal{F}_{G,\mathcal{D}}(\omega)+\mathcal{F}_{G,\mathcal{C}}(\omega)] \times\left(\frac{4\pi\cos^2\eta}{\Delta}\frac{C_\mu}{C_\Sigma}\right)^2\frac{N_1^3N_2^3}{N^6}. \tag{27}$$

Here the functions $\mathcal{F}_U(\omega),\mathcal{F}_G(\omega)$ are finite-frequency generalizations of Eq. (24)

$$\mathcal{F}_{U,\lambda}(\omega) = \left(\frac{\Delta T}{\hbar^2\omega}\right)^2 \int \tau_\lambda d\tau \frac{e^{-\pi/\tau_\lambda}\sin^2\omega\tau/2}{2\sinh^2\pi T\tau/\hbar}\frac{1}{1+\omega^2\tau_{\mathrm{RC}}^2} \times\left(1+\mathrm{Re}\,\frac{1+i\omega\tau_{\mathrm{RC}}}{1-i\omega\tau_{\mathrm{RC}}}\frac{e^{i\omega\tau}}{1-i\omega\tau_\lambda}\right), \tag{28}$$

$$\mathcal{F}_{G,\lambda}(\omega) = \left(\frac{\Delta T}{\hbar^2\omega^2}\right)^2 \int \frac{2d\tau}{\tau_\lambda}\frac{e^{-\pi/\tau_\lambda}\sin^4\omega\tau/2}{\sinh^2\pi T\tau/\hbar}. \tag{29}$$

The subscripts $U(G)$ of $\mathcal{F}_{U(G)}(\omega)$ illustrate the origin of these functions: They result from averaging of different scattering properties over the energy band defined by $\max\{\hbar\omega,T,\hbar/\tau_{\mathcal{C}(\mathcal{D})}\}$. The function $\mathcal{F}_U(\omega)$ is a characteristic of the internal potential U_ω; see Eq. (9). The function $\mathcal{F}_G(\omega)$ results from the energy averaging of the dc conductance $g(\varepsilon)$. Such averaging appears because both $G(\omega)$ defined in Eq. (10) and $g(\varepsilon)$ in Eq. (11) are coupled to the Fermi distribution.

The function $X(\omega)$ is

$$X(\omega) = \frac{N^2}{2N_1N_2}\left(\frac{(C_0\tan\eta+C_2-C_1)(1+\omega^2\tau_d\tau_{\mathrm{RC}})}{(1+\omega^2\tau_{\mathrm{RC}}^2)\nu_s e^2/\Delta} + \frac{N_2-N_1}{N(1+\omega^2\tau_{\mathrm{RC}}^2)}\right)^2, \tag{30}$$

and in the static limit $\omega\to 0$ it is given by Eq. (25). We point out that when the interactions are negligible, $E_c\sim e^2/C\ll\Delta$, the role of the bias mode is significant. A quantum dot with (fully broken) time-reversal symmetry can be labeled by Dyson symmetry parameter ($\beta=2$) $\beta=1$. When the setup is ideal, $C_{1,2}=0$, and $\eta\neq 0$, the fluctuations of $\mathcal{G}_a,\mathcal{G}_s$ at large frequencies $\omega\tau_d\gg 1$ are

$$\delta\mathcal{G}_s = \langle\mathcal{G}_s^2\rangle^{1/2} = \frac{N_1N_2}{N^2}\left(\frac{2}{\beta}\frac{\pi}{\omega\tau_d}\right)^{1/2}\frac{2\sin 2\eta}{\hbar\omega}, \tag{31}$$

$$\delta\mathcal{G}_a = \left(\frac{N_1N_2}{N^2}\right)^{3/2}\frac{\nu_s e^2}{2C}\frac{\cos^2\eta}{\hbar^2\omega^3\tau_d}, \quad \beta=2. \tag{32}$$

In chaotic quantum dots the role of the Thouless energy E_{Th} of the open systems is often played by the escape rate $\hbar/\tau_d$. If we take this into account, our result (31) qualitatively agrees with that of Falko and Khmelnitskii[20] obtained for open diffusive metallic junctions. However, when $\eta\to 0$, the fluctuations of $\mathcal{G}_s$ are much smaller and for $|N_1-N_2|\ll\omega\tau_d$ they become comparable with those of the antisymmetric conductance (32).

However, very often experiments are performed in samples, where the interaction is not weak. Since $\mathcal{G}_a$ and $\mathcal{G}_s$ are comparable for strong Coulomb interactions in the static limit $\omega\to 0$,[16] we concentrate here on this experimentally relevant regime of $\Delta/E_c\sim\tau_{\mathrm{RC}}/\tau_d\ll 1$ and take an ideal symmetric setup, $N_1=N_2$ and $C_{1,2}=0$. Then we have

TABLE I. Asymptotes of $\mathcal{F}_{U,\lambda}(\omega), \mathcal{F}_{G,\lambda}(\omega)$, and $X(\omega)$ at $T \to 0$.

Function	Adiabatic $\omega \ll \tau_\lambda^{-1}$	Intermediate $\tau_\lambda^{-1} \ll \omega \ll \tau_{RC}^{-1}$	High $\omega\tau_{RC} \gg 1$
$\mathcal{F}_U(\omega) \times N_\lambda^2$	1	$\pi/(4\omega\tau_\lambda)$	$\pi/(4\omega^3\tau_\lambda\tau_{RC}^2)$
$\mathcal{F}_G(\omega) \times N_\lambda^2$	1	$(\pi/\omega\tau_\lambda)^3$	
$X(\omega)$	$2\tan^2\eta(\tau_{RC}/\tau_d)^2$		$2\tan^2\eta$

$$X(\omega) \approx 2\tan^2\eta\left(\frac{\tau_d^{-1} + \omega^2\tau_{RC}}{\tau_{RC}^{-1} + \omega^2\tau_{RC}}\right)^2. \tag{33}$$

Below we consider in detail the case $\eta \neq 0$ and how this bias mode affects the behavior of $\mathcal{G}_s^2(\omega)$. Several frequency regimes can be separated: Adiabatic $\omega\tau_\lambda \ll 1$, intermediate, where $1/\tau_\lambda \ll \omega \ll 1/\tau_{RC}$, and high frequencies $\omega\tau_{RC} \gtrsim 1$. The asymptotes of the functions defined in Eqs. (28), (29), and (33) in these regimes are presented in Table I for reference.

For adiabatic frequencies $\omega\tau_\lambda \ll 1$ the integrands in Eqs. (28) and (29) do not oscillate on the short time scale τ_λ. At such small frequencies $\mathcal{F}_U(\omega) = \mathcal{F}_G(\omega)$ are equal to $\mathcal{F}$ of Eq. (24) and $X(\omega) \propto (\tau_{RC}/\tau_d)^2 \ll 1$ can be neglected. This is essentially the zero frequency regime considered before for nonlinear dc transport.

As the frequency grows, an intermediate regime is reached when $\max\{T, \hbar/\tau_\lambda\} \ll \hbar\omega \ll \hbar/\tau_{RC}$ and $\mathcal{F}_U(\omega), \mathcal{F}_G(\omega)$ start to differ. The scattering properties at large energy difference $\hbar\omega \gg \hbar/\tau_\lambda$ are uncorrelated and the response of the dot is randomized. Therefore both the conductance averaged over a large energy window $\hbar\omega$ and the response of the internal potential U_ω to the ac voltage at $\omega\tau_d \gg 1$ are strongly suppressed; see Table I. As a result, if $X(\omega)$ is still negligible, both $\mathcal{G}_a^2$ and $\mathcal{G}_s^2$ decrease with growing frequency as $1/\omega^4$.

One could expect that interactions qualitatively change the behavior of $\mathcal{G}_a, \mathcal{G}_s$ when the frequencies become comparable to $1/\tau_{RC} \sim NE_c/\hbar$, the scale defined by the interaction strength. At such frequencies the response of a dot to the potentials at the contacts is not resistive as occurs at low frequencies, but mostly capacitive. If the frequency is high, $\omega\tau_{RC} \gtrsim 1$, we have $\mathrm{Re}\, u_{1,2} \to 0$ and the function $\mathcal{F}_U$ in Eq. (28) is suppressed $\sim 1/(\omega\tau_{RC})^2$. As a consequence, $\mathcal{G}_a^2$ is suppressed stronger then $1/\omega^4$ and goes as $1/\omega^6$ at $\omega\tau_{RC} \gtrsim 1$. However, a more important signature of this capacitive coupling is the growth of $X(\omega)$ in Eq. (33), which affects $\mathcal{G}_s^2$.

To see the role of this growth we consider now sufficiently large fields $\Phi = \Phi'$ when only the diffuson contribution survives. The growth of $X(\omega)$ in Eq. (33) reflects enhanced sensitivity of the internal potential U_ω to the gate voltage, $X(\omega) \propto (\tan\eta\, \mathrm{Re}\, u_0)^2$. At high frequencies the impedance of the capacitor C becomes negligible and therefore the internal potential follows the gate voltage and not the reservoir voltages, $u_0 \to 1, u_{1,2} \to 0$. Enhanced from its small static value τ_{RC}/τ_d to 1 at large frequencies, such coupling affects the fluctuations of $\mathcal{G}_s(\omega)$ if $\eta \neq 0$. The situation is somewhat similar to the weak interaction limit, when the coupling with nearby gates was strong, $u_0 \to 1, u_{1,2} \ll 1$, and lead to $\mathcal{G}_s \gg \mathcal{G}_a$.

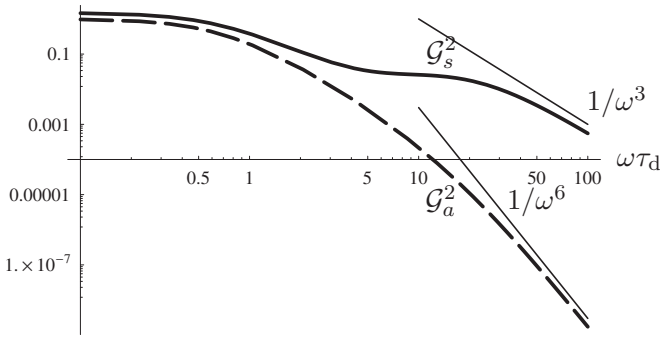

FIG. 4. Zero-temperature large-field fluctuations of $\mathcal{G}_a(\omega)$ (dashed) and $\mathcal{G}_s(\omega)$ (solid curve) in units of $(\pi/4\Delta N^2)^2$ for the bias mode $\eta = \pi/4$. Data are presented in the log-log scale at $N_{1,2} = 5$ and $\tau_{RC}/\tau_d = 0.05$. The asymptotes $\mathcal{G}_a^2 \propto \omega^{-6}$ and $\mathcal{G}_s^2 \propto \omega^{-3}$ are different due to $\eta \neq 0$; see Eqs. (34) and (35).

The fluctuations of $\mathcal{G}_a(\omega), \mathcal{G}_s(\omega)$ for $\omega\tau_d \gg 1$ can be evaluated:

$$\mathcal{G}_a^2(\omega) \sim \frac{\Delta^2}{(\hbar\omega)^4(1 + \omega^2\tau_{RC}^2)}, \tag{34}$$

$$\mathcal{G}_s^2(\omega) \sim \mathcal{G}_a^2(\omega) + \frac{(\tau_{RC}\tan\eta[1 + \omega^2\tau_d\tau_{RC}])^2}{\hbar^2\omega\tau_d(1 + \omega^2\tau_{RC}^2)^3}. \tag{35}$$

Fluctuations of $\mathcal{G}_a^2(\omega)$ and $\mathcal{G}_s^2(\omega)$ demonstrate qualitatively different behavior, which we illustrate in Fig. 4. Indeed, at sufficiently high frequencies, the dependence of $X(\omega)$ on ω makes the last term in Eq. (35) dominant. At $\omega\tau_{RC} \gg 1$ the asymptotes of $\mathcal{G}_a^2 \propto 1/\omega^6$ and $\mathcal{G}_s^2 \propto 1/\omega^3$ become different due to the presence of the second term in Eq. (35). These results show that for nonadiabatic frequencies of the external bias the dc current strongly depends on the bias mode η. We predict that the magnetic field asymmetry of the rectified current, noticeable at small frequencies, might become suppressed for large frequencies, when the symmetrized component dominates due to the presence of capacitive coupling. For convenience, the low-temperature estimates for $\langle\mathcal{G}_a^2\rangle$ and $\langle\mathcal{G}_s^2\rangle$ for $\eta \neq 0$, $\Phi \gg \Phi_c$ are collected in Table II.

It is noteworthy that a recent experiment in AB rings[12] finds that $\mathcal{G}(\omega, \Phi = 0)$ grows with frequency until $\omega \sim 2E_{Th}$ and then decreases $\sim 1/\omega^{3/2}, \omega \to \infty$. While we predict a monotonic decrease of $\langle\mathcal{G}_s^2(\omega)\rangle$, this growth could be the result of quantum pumping or an interference of the pumping and rectification (both effects were neglected here).

TABLE II. Estimates for $\langle\mathcal{G}_a^2\rangle$ and $\langle\mathcal{G}_s^2\rangle$ ($z = \omega\tau_d$).

Function	Adiabatic $z \ll 1$	Intermediate $1 \ll z \ll \tau_d/\tau_{RC}$	High $z \gg \tau_d/\tau_{RC}$
$\frac{\hbar^4}{\Delta^2\tau_d^2}\mathcal{G}_a^2$	1	z^{-4}	$\frac{\tau_d^2}{\tau_{RC}^2}z^{-6}$
$\frac{\hbar^2}{\tau_{RC}^2}(\mathcal{G}_s^2 - \mathcal{G}_a^2)$	1	$\left(1 + \frac{\tau_{RC}}{\tau_d}z^2\right)^2 z^{-1}$	$\frac{\tau_d^3}{\tau_{RC}^4}z^{-3}$

VI. PHASE OF AHARONOV-BOHM OSCILLATIONS

In this section, we consider nonlinear transport through a chaotic Aharonov-Bohm (AB) ring. The nonlinear conductance $\mathcal{G}$ exhibits periodic AB oscillations and nonperiodic fluctuations, similarly to the linear conductance G. However, since Coulomb interactions produce asymmetry of $\mathcal{G}$ with respect to magnetic field inversion, the phase of these oscillations is not pinned to 0 (mod)π. As a quantum effect this AB phase is characterized by a mesoscopic distribution. The width of this distribution represents a typical fluctuation. We first discuss what kind of distribution could be expected in a chaotic AB ring and then calculate the fluctuation of the AB phase.

Let us assume that $\mathcal{G}$ as a function of magnetic flux Φ can be expanded into the series of well-defined Fourier harmonics similarly to the linear conductance G:

$$\begin{Bmatrix} G(\Phi) \\ \mathcal{G}(\Phi) \end{Bmatrix} = \sum_{n=0}^{\infty} \begin{Bmatrix} G_n \\ \mathcal{G}_n \end{Bmatrix} \cos\left(\frac{2\pi n \Phi}{\Phi_0} + \begin{Bmatrix} 0 \\ \delta_n \end{Bmatrix} \right). \tag{36}$$

The phase δ of the main (first) harmonic $\Phi_0 = hc/e$ is obtained from the ratio of the (anti)symmetrized conductances defined in Eq. (2)

$$\tan \delta = \frac{\int d\Phi \exp(2\pi i \Phi/\Phi_0) \mathcal{G}_a(\Phi)}{\int d\Phi \exp(2\pi i \Phi/\Phi_0) \mathcal{G}_s(\Phi)}. \tag{37}$$

We can not find the full mesoscopic distribution of the phase $P(\delta)$. We can gain some insight in the behavior of this phase by investigating a similar quantity, namely, the asymmetry parameter $\mathcal{A} = \mathcal{G}_a/\mathcal{G}_s$ considered previously for chaotic dots.[16] Based on Eq. (37) we argue that the statistical properties of arctan $\mathcal{A}$ and the AB phase δ should be similar.

In quantum dots the parameter $\mathcal{A}$ is given by the ratio $\mathcal{A} = \mathcal{G}_a/\mathcal{G}_s = \chi_{2a}/\chi_{2s}$; see Eqs. (16), (18), and (19). The functions $\chi_{2a,2s}$ at $T \neq 0$ are convolved separately with $f'(\varepsilon)$, and at $T=0$ (which we consider below) they are evaluated at the Fermi energy. The properties of $\chi_{2a,2s}$ and the dependence of χ_{2s} on the bias mode were described after Eq. (25). The function χ_{2s} can have a nonzero (classical) average $\langle \chi_{2s} \rangle \sim X^{1/2}$ defined by the interaction strength, geometry of the set-up, and the bias mode η. Since $\langle \chi_{2,a} \rangle = 0$ and the fluctuations of $\chi_{2a,2s}$ are small as $1/N^2$, the mesoscopic distribution of arctan $\mathcal{A}$ is narrow and concentrated close to 0. However, $\langle \chi_{2s} \rangle = 0$ is possible if $X \to 0$, e.g., for symmetric contacts and the bias mode $\eta = 0$. In this case, the distribution of arctan $\mathcal{A}$ becomes wide regardless of the interaction strength.

The role of the classical contribution on the shape of $P(\arctan \mathcal{A})$ is demonstrated in the main plot in Fig. 5 for $\eta = 0$, where the distributions for asymmetric, $N_L = 4, N = 16$, and symmetric contacts, $N_L = 8, N = 16$, are presented. While the distribution is almost uniform, when the classical contribution X is absent, it is highly peaked near zero when X dominates. If X is absent, the correlations between $\mathcal{G}_a$ and $\mathcal{G}_s$ are significant at small N. This leads to a nonuniform distribution of $P(\arctan \mathcal{A})$, which is peaked at 0 and $\pi/2$ when $N=2$; see the inset in Fig. 5. When N grows, the correlations

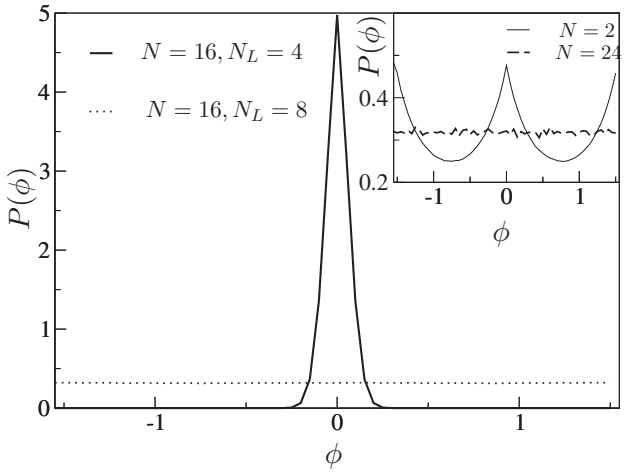

FIG. 5. Mesoscopic distribution $P(\phi)$ of $\phi = \arctan \mathcal{G}_a/\mathcal{G}_s$. (Main plot) If the contacts are asymmetric (bold curve, $N=16, N_L=4$) the distribution is narrow, while for symmetric contacts (dashed, $N=16, N_L=8$) it is almost uniform. As shown in the inset, for symmetric contacts at large N the distribution becomes uniform; compare bold curve for $N=2$ and dashed for $N=24$.

between $\mathcal{G}_a$ and $\mathcal{G}_s$ vanish and therefore the distribution becomes uniform. Such a distribution could be easily obtained if we make the natural assumption that $\mathcal{G}_a, \mathcal{G}_s$ are independent and distributed by the Gaussian law with the same width.

These numerics were performed for $\eta = 0$, when the mesoscopic distribution of $\mathcal{A} = \mathcal{G}_a/\mathcal{G}_s$ becomes insensitive to the interaction strength. The role of interactions appears only if $\eta \neq 0$, when the classical contribution X becomes dominant. Similarly, we expect that the distribution of the phase of AB oscillations is also strongly affected by the bias mode. If the bias mode is chosen such that the classical contribution X vanishes, the phase δ strongly fluctuates *even for weak interactions*. It would be very interesting to check this surprising conclusion experimentally.

Let us now consider the fluctuations of the AB phase. Since the scattering theory turned out to be very useful for the discussion of the nonlinear/rectified current through a chaotic quantum dot, we extend this theory to rings. We make two key assumptions (discussed in the Appendix in more detail) that the magnetic flux through the annulus of the ring is smaller then the flux quantum Φ_0 and that the mean free path l, the radius R, the width of the ring W and the contacts W_c satisfy the condition $\pi^2 l W \gg 2 R W_c$. In this case the RMT can be applied to such chaotic rings as well. Unlike the experiments on large open rings with high aspect ratio $R/W \gg 1$,[2,22–25] the recent experiments[9,11,12] are performed in rings of submicron size, which are effectively zero-dimensional. The treatment of such rings is similar to chaotic quantum dots, and the fluctuations of $\mathcal{G}_s, \mathcal{G}_a$ can be expressed in terms of the diffuson $\mathcal{D}$ and the Cooperon $\mathcal{C}$; see Eq. (23). The only problem is to find the expression for the effective number of channels as a function of magnetic field, similar to Eq. (21).

The model we propose for a chaotic AB ring combines chaos and a ring geometry: A chaotic dot is attached to a long ballistic arm which serves to include an AB flux large

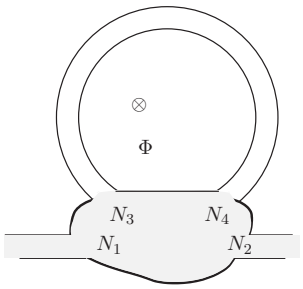

FIG. 6. Model of a chaotic Aharonov-Bohm ring with $N=N_1+N_2$ channels. The model consists of a quantum dot with M channels combined with a ballistic arm with $N_3=N_4=(M-N)/2$ channels.

compared to the fraction of the flux through the sample. This model is shown in Fig. 6, where the ring with $N=N_1+N_2$ ballistic channels in the contacts 1,2 is modeled by a dot with $M>N$ channels and a ballistic arm with $N_3=N_4=(M-N)/2$ channels in contacts 3,4. The parameter $\rho=1-N/M$, the ratio of N_3+N_4 to the total number of channels M, can vary between 0 when the arm is much narrower then the contacts and 1 in the opposite limit. The electronic phase is randomized in the quantum dot, but when electrons propagate along the arm their phase is determined by the geometry and applied magnetic field. This model is a reasonable approximation for the real experiment; it takes into account the long time spent by electrons inside the ring and the randomness of its motion. The discussion of the model and the details of calculation of $\mathcal{C},\mathcal{D}$ are presented in the Appendix.

In experiment, the Fourier transform is often taken over the total flux (or applied magnetic field) and the flux through the hole Φ_h cannot be separated from the flux through the dot Φ_d. Then the dependence of the diffuson and Cooperon on magnetic field is nonperiodic, which is indeed observed in the form of non-periodic fluctuations in the (non)linear conductance and phase slips of AB oscillations. A possible weakness of this model is in its spatial separation of chaotic scattering and the main part of magnetic field, but in the limit when the arm is much wider then the contacts 1 and 2 such a separation is not important and the averaged properties of AB-oscillation phase become independent of the arm's width.

If the flux Φ_d through the dot is much smaller then the flux Φ_h through the hole, the nonperiodic fluctuations and the periodic AB oscillations are well-separated, which is usually the case in experiment.[9,11] In view of this separation we can neglect the flux through the chaotic dot, $\Phi_d \ll \Phi_h$, to find the statistics of the AB phase. We assume that the averaging is taken over a magnetic field range containing many AB oscillations but still small compared to the characteristic field of the nonperiodic fluctuations. In such a simplified model of a chaotic AB ring $N_{\mathcal{C},\mathcal{D}}$ are given by Eq. (A6) with $\Phi_d=0,\Phi_h=\Phi$ and the parameter $\rho=(M-N)/M$. The effective number of channels is

$$\begin{Bmatrix} N_{\mathcal{C}} \\ N_{\mathcal{D}} \end{Bmatrix} = M\left(1-\rho\cos\frac{2\pi(\Phi\pm\Phi')}{\Phi_0}\right). \tag{38}$$

Using this expression for the $N_{\mathcal{C},\mathcal{D}}$ we can evaluate the quantum fluctuations of linear conductance in AB rings. At low temperature a typical fluctuation of G at $\Phi=0$ is $\delta G=\sqrt{2}(N_1N_2/N^2)(\nu_s e^2/h)$ and the amplitude of AB oscillations is $\delta G_{\mathrm{AB}}^2 \sim \delta G^2\rho(1-\rho)^{1/2}/(1+\rho)^{3/2}$, which reaches maximum when the widths of the arm and the contacts are equal, $\rho=1/2$.

The first two moments of $\tan\delta$ can be found analytically. It is zero on average, $\langle\tan\delta\rangle=0$, since the numerator and denominator in Eq. (37) are independent random quantities. Equation (38) show that $\mathcal{D},\mathcal{C}$ are the same functions of $\Phi\pm\Phi'$, so that all necessary ingredients can be expressed in terms of the functions $\mathcal{F}_{U,\mathcal{D}}$ and $\mathcal{F}_{G,\mathcal{D}}$ of $\Phi-\Phi'$ defined in Eqs. (28) and (29). We omit now the index $\mathcal{D}$ for brevity and denote the average over magnetic field by $\overline{(\ldots)}=\int_0^{\Phi_0}(\ldots)d\Phi/\Phi_0$, to find

$$\langle\tan^2\delta\rangle = [\overline{\mathcal{F}_U(\Phi)\mathcal{F}_G(\Phi)\cos\Phi} + \overline{\mathcal{F}_G}\cdot\overline{\mathcal{F}_U(\Phi)\cos\Phi} - \overline{\mathcal{F}_U}\cdot\overline{\mathcal{F}_G(\Phi)\cos\Phi}] \Big/ \left(\overline{[\mathcal{F}_U(\Phi)+X(\omega)]\mathcal{F}_G(\Phi)\cos\Phi} + \frac{\overline{\mathcal{F}_U(\Phi)}}{2}\overline{\mathcal{F}_G(\Phi)\cos\Phi} + \frac{\overline{\mathcal{F}_G(\Phi)}}{2}\overline{\mathcal{F}_U(\Phi)\cos\Phi}\right), \tag{39}$$

where the function $X(\omega)$ is defined by the set-up geometry in Eq. (33). Again, in the static limit $\omega\to 0$ we have $\mathcal{F}_U=\mathcal{F}_G=\mathcal{F}$ and X defined by Eqs. (24) and (25). In this case Eq. (39) can be rewritten as

$$\frac{1}{\langle\tan^2\delta\rangle} = 1 + \frac{[\overline{\mathcal{F}(\Phi)}+X]\overline{\cos\Phi\mathcal{F}(\Phi)}}{\overline{\cos\Phi\mathcal{F}^2(\Phi)}}. \tag{40}$$

In the limits of high, $T\gg N\Delta/2\pi$, and low, $T\ll N\Delta/2\pi$, temperature, the asymptotical values of $\langle\tan^2\delta\rangle$ are

$$\frac{1}{\langle\tan^2\delta\rangle} = 1 + \begin{cases} \dfrac{\sqrt{1-\rho^2}}{1+\sqrt{1-\rho^2}} + \dfrac{12T}{\Delta}\dfrac{XM(1-\rho^2)}{1+\sqrt{1-\rho^2}}, & T\gg\dfrac{N\Delta}{2\pi}, \\ \dfrac{2\sqrt{1-\rho^2}}{4+\rho^2} + \dfrac{2XM^2(1-\rho^2)^2}{4+\rho^2}, & T\ll\dfrac{N\Delta}{2\pi}. \end{cases}$$

Very important is the case of symmetric contacts, $N_1=N_2$,

and antisymmetric bias mode, $\eta=0$, which is used in Ref. 9. Then X vanishes and the average $\tan^2\delta$ becomes independent of interaction strength and as a function of T it is very weak. That is not the case if $\eta\neq 0$; for example, when only one of the voltages changes, $\eta=\pm\pi/4$.[11,12] Then the statistics of the AB phase becomes temperature and interaction dependent due to the presence of X.

The limit $M\gg N$ corresponds to a uniformly chaotic ring, which we suppose to be closer to the experimental situation. Then the dependence on M drops out and the high/low temperature asymptotic reads

$$\frac{1}{\langle\tan^2\delta\rangle}=1+8X\begin{cases}3NT/\Delta, & T\gg N\Delta/2\pi,\\ N^2/5, & T\ll N\Delta/2\pi.\end{cases} \tag{41}$$

This result clearly demonstrates that the phase of the oscillations is expected to deviate strongly from 0, especially if the temperature is low and the number of channels in the contacts is diminished. The temperature is taken into account only in the form of temperature-averaging and the dephasing (previously considered for nonlinear transport of noninteracting electrons in Refs. 51–53) is not included.

We expect our model for chaotic AB rings to work both for experiments at small frequencies[9,11] and for large frequencies.[12] Similarly to quantum dots, the generalization on the finite-frequency case is obvious, if we use Eq. (33). Even in cases where RMT cannot be assured to be valid for open diffusive rings, the dependence of the AB phase on interaction strength, temperature, and number of external channels given by Eq. (41) should be correct qualitatively.

The experiment of Leturcq *et al.*[9] is performed in a bias mode $\eta=0$ when $X=0$. Then Eq. (41) gives $\langle\tan^2\delta\rangle=1$. The phase of the oscillations is evaluated from data according to Eq. (37) over a large range of fields. In experiment the AB phase is varied continuously as a function of the gate voltage at one of the arms of the ring. The data demonstrate that the phase δ indeed changes in a wide range and is usually far from 0. This substantiates our conclusion that in the mode when the classical contribution is minimized, $X\to 0$, the mesoscopic distribution of δ is very wide.

The experiment of Angers *et al.*[11] varies voltage in a different way, $\eta=\pi/4$, and therefore has $X\neq 0$. We would expect the phase $\delta(\mathrm{mod})\pi$ to take values closer to 0 and the antisymmetric component of the oscillations be relatively smaller even for large fields. Although phases close to 0 are indeed observed, the field averaging is taken only over the first few oscillations. In this range $\mathcal{G}_a$, the numerator in Eq. (37) is still small and grows linearly with magnetic field. Averaging over a larger field-range similar to Ref. 9 could not be performed because of the phase slips.

Another interesting question is a difference in data[9,11] for the relative magnitudes $\mathcal{G}_2/\mathcal{G}_1$ of the Second $hc/2e$ and main harmonic hc/e; see Eq. (36). In the nonlinear transport regime this harmonic is small compared to its contribution in the linear transport, $\mathcal{G}_2/\mathcal{G}_1\ll G_2/G_1$,[9] while in Ref. 11 they were comparable, $\mathcal{G}_2/\mathcal{G}_1\approx G_2/G_1$. Our model also predicts the mesoscopically averaged contribution of $hc/2e$ into linear and nonlinear conductance to be comparable with that of hc/e. Our approach assumes full quantum coherence of the ring, and probably the difference in data is due to decoherence.

VII. CONCLUSIONS

In this paper, we consider mesoscopic chaotic samples (quantum dots or rings) and find the statistics of their nonlinear conductance $\mathcal{G}$. This transport coefficient characterizes nonlinear dc current due to dc bias or a rectified current due to ac bias or photon-assisted transport. For chaotic samples, the nonlinear effect is of quantum origin, which is clear from the fact that its ensemble average over similar samples vanishes. The linear response of the sample in two-terminal measurements is always symmetric with respect to magnetic field inversion. However, the Coulomb interactions lead to magnetic field asymmetry of the nonlinear dc response, which fluctuates due to the electronic interference. For the quantum dots we consider the fluctuations of (anti) symmetrized components $\mathcal{G}_a,\mathcal{G}_s$ of the nonlinear conductance. In chaotic rings the statistics of the phase of AB oscillations in the nonlinear transport regime, closely related to the ratio $\mathcal{G}_a/\mathcal{G}_s$, is of interest.

Unlike the linear conductance measurements, in mesoscopic nonlinear transport experiments the way voltages are varied ("bias mode") turns out to be important, especially for a weakly interacting sample. We demonstrate this fact qualitatively and discuss the role of Coulomb interactions. Quantitative self-consistent treatment of interactions allows us to consider magnetic-field asymmetry in chaotic quantum dots with many channels. Using Eqs. (23)–(25) we show that the fluctuations of $\mathcal{G}_s$ are strongly affected by the geometry of the setup and discuss how the bias mode influences data of recent dc experiments.

Another important issue is rectification of ac bias, which is quadratic in applied voltage, random, and asymmetric with respect to the magnetic flux inversion. The photovoltaic dc current can be due to rectification of external perturbations or quantum pumping by internal perturbations. Both rectification and quantum pumping share the aforementioned properties, and it is important to clearly separate them especially when the frequency of perturbations is high (nonadiabatic). We consider here only the effects of the external perturbations and discuss the dependence of the fluctuations of $\mathcal{G}_a,\mathcal{G}_s$ on frequency ω. We show that the fluctuations of both $\mathcal{G}_a$ and $\mathcal{G}_s$, presented in Eqs. (27)–(30), decrease monotonically as $\omega\to\infty$. However, contrary to naive expectations, their asymptotical behavior can be very different. Since at high frequencies the response of the dot to the external bias becomes rather capacitive then resistive, the coupling to the nearby gates can be strongly enhanced. If the experiment is performed in a bias mode where such coupling contributes, the symmetrized $\mathcal{G}_s^2(\omega)\propto 1/\omega^3$ can become much larger then $\mathcal{G}_a^2(\omega)\propto 1/\omega^6$ valid for a strongly interacting quantum dot. The same conclusion holds in the weakly interacting limit, when $\mathcal{G}_s^2\propto 1/\omega^{3/2}$ and $\mathcal{G}_a^2\propto 1/\omega^3$.

In addition, we show that recent experiments in chaotic Aharonov-Bohm rings might be considered similarly to quantum dots. The multiply connected geometry alone leads

to AB oscillations, yet the mesoscopic distribution of their phase is expected to be qualitatively similar to that of $\arctan \mathcal{G}_a/\mathcal{G}_s$ in quantum dots. Therefore, the bias mode should strongly affect the shape of mesoscopic distribution of the AB phase. The model of an AB ring, which we develop, consists of a dot and a long ballistic arm and takes into account both chaos and a ring geometry. As an application of our model we consider fluctuations of the AB phase. Unlike the AB phase in the linear conductance, pinned to $0(\mathrm{mod})\pi$ by the Onsager symmetry relations, the fluctuations of the AB phase in nonlinear transport are shown to depend on the bias mode, interaction strength, and temperature.

ACKNOWLEDGMENTS

We thank Hélène Bouchiat, Piet Brouwer, Renaud Leturcq, David Sánchez, Maxim Vavilov, and Dominik Zumbühl for valuable discussions. We also thank the authors of Ref. 12 for sharing their results with us before publication. This work was supported by the Swiss National Science Foundation, the Swiss Center for Excellence MaNEP, and the STREP project SUBTLE.

APPENDIX: DIFFUSON AND COOPERON FOR CHAOTIC RING

In this appendix we determine the diffuson and Cooperon contributions to the $\mathcal{S}$-matrix correlators of the random scattering matrix of a chaotic Aharonov-Bohm (AB) ring. This calculation is performed using random matrix theory (RMT).

First we explain what approximations should be made to ensure validity of RMT. Our starting point is the assumption that the $\mathcal{S}$-matrix of the ring is uniformly distributed over the unitary group. This means that the ring is essentially zero-dimensional, similarly to quantum dots. RMT is applicable if all energy-scales are much smaller then the Thouless energy E_{Th} and the total flux through the annulus of the ring is much smaller then Φ_0. Assume the ring of radius R and width $W \ll R$ to be diffusive with diffusion coefficient $D=lv_F/2$. To evaluate E_{Th} we neglect with transversal motion of an electron and find $E_{\mathrm{Th}}=\hbar/\tau_{\mathrm{erg}}=(\hbar l v_F)/2R^2$ as a solution to Laplace equation along the circumference of the ring. RMT can be applied to a closed ring if the dimensionless conductance is large, $g=E_{\mathrm{Th}}/\Delta=k_F l W/2R \gg 1$, which is usually satisfied for a weak disorder even if $W \ll R$.

An open ring with ballistic contacts of the width W_c gains a new energy parameter, the escape rate $\hbar/\tau_d=N\Delta/2\pi$, where N is the total number of ballistic channels. The scattering matrix $\mathcal{S}$ is uniformly distributed and independent of the exact positions of the contacts (and therefore the length of the arms) if $\hbar/\tau_d \ll E_{\mathrm{Th}} \Rightarrow \pi^2 l W \gg 2RW_c$. In this case the main drop of the potential occurs in the contacts.

If a magnetic field is applied, the RMT is valid if the total flux through the annulus of the ring is much less then the flux quantum, $\Phi \ll \Phi_0$. Due to narrow contacts the time-reversal symmetry (TRS) of the $\mathcal{S}$-matrix can be broken at a much smaller scale, $\Phi \sim \Phi_0 \sqrt{\tau_{\mathrm{erg}}/\tau_d}$. Since in our rings $\tau_{\mathrm{erg}} \ll \tau_d$, a full crossover to the broken TRS can be considered.

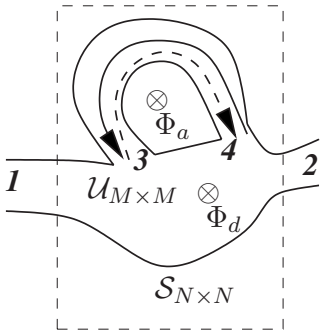

FIG. 7. Chaotic dot combined with long ballistic multichannel arm.

How well are these conditions fulfilled in the experiment? In Ref. 9 chaos was mainly due to diffusive scattering on the boundary and $l \approx R$. The width of the arm is 2–4 channels, while the number of channels in the contacts is $N \sim 2$, estimated from the linear conductance measurements, so $\tau_d/\tau_{\mathrm{erg}} \sim 5-10 \gg 1$. In semiballistic samples of Ref. 11 (obtained by etching, and therefore having diffusive boundary scattering) $W=W_c$ and the mean free path is estimated $l \sim 1-2\ \mu\mathrm{m} \sim L=1.2\ \mu\mathrm{m}$, the side length. Therefore, we have a similar estimate for the ratio $\tau_d/\tau_{\mathrm{erg}}$. Although this ratio is not parametrically large due to, e.g., weak disorder $k_F l \gg 1$, we believe that such AB rings still can be assumed zero-dimensional due to their good conducting properties together with relatively narrow contacts.

In our calculations we make a further simplification by spatially separating chaotic scattering which randomizes the electronic phase and the long ballistic arm attached to it. To find the correlators of the $\mathcal{S}$-matrix elements we use a simplified model, see Fig. 7, which combines chaos and a ring geometry. A chaotic M-channel dot is attached to a long multichannel ballistic arm with $(M-N)/2$ orbital channels. We assume that the size of the dot L and the length of the arm L_a are such that $L_a \gg L \gg \sqrt{(M-N)\lambda_F L_a}$ to ensure that in the hierarchy of different fluxes the main flux Φ_h is concentrated in the region embraced by the arm, the flux through the dot Φ_d is much smaller, but still much larger then the flux through the cross section of the arm. The amplitude of AB oscillations depends on the width of the arm $\propto(M-N)$. The wider the arm (relatively to the contacts) the closer the results should be to a uniformly chaotic ring. For the case when $M \gg N$ we expect it to be valid for the chaos uniformly distributed over the ring. Indeed, in this case an electron makes $\sim M/N \gg 1$ windings around the arm before exiting.

In this appendix it is more convenient for us to work with an energy-dependent matrix $\mathcal{S}(\varepsilon)$, and the final transformation to time-representation is rather obvious. The total scattering matrix $\mathcal{S}$ is of size $N \times N$ due to scattering channels in the contacts 1 and 2. Chaotic scattering in the M-channel quantum dot is characterized by the $M \times M$ matrix $\mathcal{U}$. The scattered electron can either exit the sample through the $N=N_1+N_2$ channels (projection operator $P_0=1_1 \oplus 1_2$) or propagate into the arm with $N_3=N_4=(M-N)/2$ channels. Electrons propagate through this arm ballistically and gain phases which depend on the flux through the hole. In the absence of backscattering the electronic amplitudes at energy ε are re-

lated to the path length L_a and magnetic field phase ϕ:

$$\begin{pmatrix} b_3 \\ b_4 \end{pmatrix} = e^{-ik(\varepsilon)L_a} \begin{pmatrix} 0 & e^{-i\phi} \\ e^{i\phi} & 0 \end{pmatrix} \begin{pmatrix} a_3 \\ a_4 \end{pmatrix} = P \begin{pmatrix} a_3 \\ a_4 \end{pmatrix}. \quad \text{(A1)}$$

The scattering matrix of the arm is $\mathcal{P}(\varepsilon)=0_1 \oplus 0_2 \oplus P$. Each time an electrons enters the arm either through the third or fourth lead, the matrix $\mathcal{P}$ contributes to the scattering amplitude of the process. The total scattering matrix $\mathcal{S}$ is determined from the following equation:

$$\mathcal{S} = P_0 \sum_{n=0}^{\infty} \mathcal{U}(\mathcal{P}\mathcal{U})^n P_0 = P_0 \mathcal{U} \frac{1}{1-\mathcal{P}\mathcal{U}} P_0, \quad \text{(A2)}$$

where multiple $n \geq 0$ windings are taken into account. Both $\mathcal{U}(\varepsilon,B)$, and $\mathcal{P}(\varepsilon,B)$ are field and energy dependent. Once we are interested only in pair correlators of $\mathcal{S}(\varepsilon),\mathcal{S}^{\dagger}(\varepsilon')$ for $N,M \gg 1$, the diffuson $\mathcal{D}$ and Cooperon $\mathcal{C}$ of our scattering matrix are expressed via correlators of the dot, $\mathcal{D}_{\mathcal{U}},\mathcal{C}_{\mathcal{U}}$, and $\mathrm{tr}\, \mathcal{P}(\varepsilon)\mathcal{P}^{*(\dagger)}(\varepsilon')$. The correlators of the $\mathcal{U}$-matrix are known, see Eq. (20) for their time representation, and for $\mathcal{D}$ and $\mathcal{C}$ we derive

$$\begin{Bmatrix} \mathcal{C} \\ \mathcal{D} \end{Bmatrix}^{-1} = \begin{Bmatrix} \mathcal{C}_{\mathcal{U}}^{-1} - \mathrm{tr}\, \mathcal{P}(\varepsilon)\mathcal{P}^{*}(\varepsilon') \\ \mathcal{D}_{\mathcal{U}}^{-1} - \mathrm{tr}\, \mathcal{P}(\varepsilon)\mathcal{P}^{\dagger}(\varepsilon') \end{Bmatrix}, \quad \text{(A3)}$$

$$\begin{Bmatrix} \mathcal{C} \\ \mathcal{D} \end{Bmatrix}_{\mathcal{U}}^{-1} = M - 2\pi i \frac{\varepsilon-\varepsilon'}{\Delta} + \frac{h v_F l}{L^2 \Delta} \left(\frac{\Phi_d \pm \Phi_d'}{2\Phi_0} \right)^2. \quad \text{(A4)}$$

The flux penetrating the dot is denoted as Φ_d and the phase $\phi \approx 2\pi\Phi_h/\Phi_0$ gained in the arm depends on the flux Φ_h through the hole. The traces read

$$\mathrm{tr} \begin{Bmatrix} \mathcal{P}(\varepsilon,\Phi)\mathcal{P}^{*}(\varepsilon',\Phi') \\ \mathcal{P}(\varepsilon,\Phi)\mathcal{P}^{\dagger}(\varepsilon',\Phi') \end{Bmatrix} = (M-N)\cos \begin{Bmatrix} \phi+\phi' \\ \phi-\phi' \end{Bmatrix} \times e^{iL_a[k(\varepsilon)-k(\varepsilon')]}. \quad \text{(A5)}$$

Since we assumed that the area of the arm is small compared to that of the dot, the energy dependence of Eq. (A5) can be neglected compared to that of $\mathcal{D}_{\mathcal{U}},\mathcal{C}_{\mathcal{U}}$ in Eq. (A4). We also assumed that since the arm is much longer than the size of the dot, $L_a \gg L$, the phases ϕ,ϕ' of open trajectories in the arm correspond to the flux Φ_h,Φ_h' through the hole. Therefore, the effective number of channels $N_{\mathcal{C},\mathcal{D}}$, similar to Eq. (21) for quantum dots is

$$\begin{Bmatrix} N_{\mathcal{C}} \\ N_{\mathcal{D}} \end{Bmatrix} = M - (M-N)\cos \frac{2\pi(\Phi_h \pm \Phi_h')}{\Phi_0} + \frac{h v_F l}{L^2 \Delta} \left(\frac{\Phi_d \pm \Phi_d'}{2\Phi_0} \right)^2. \quad \text{(A6)}$$

The energy-dependent Cooperon and diffuson in energy representation are given by $X(\varepsilon,\varepsilon')=1/[N_X - 2\pi i(\varepsilon-\varepsilon')/\Delta], X=\mathcal{C},\mathcal{D}$. Notice that when $\Phi=\Phi'$ the Cooperon $\mathcal{C}$ is nonperiodic in the total flux $\Phi=\Phi_h+\Phi_d$ due to finite flux through the material of the sample, $\Phi_d \neq 0$.

*polian@physics.unige.ch

[1] V. I. Belinicher and B. I. Sturman, Usp. Fiz. Nauk **130**, 415 (1980) [Sov. Phys. Usp. **23**, 199 (1980)].
[2] S. Washburn and R. A. Webb, Rep. Prog. Phys. **55**, 1311 (1992).
[3] B. L. Altshuler and D. E. Khmelnitskii, Pis'ma Zh. Eksp. Teor. Fiz. **42**, 291 (1985) [JETP Lett. **42**, 359 (1985)].
[4] D. E. Khmelnitskii and A. I. Larkin, Phys. Scr., T **T14**, 4 (1986); Zh. Eksp. Teor. Fiz. **91**, 1815 (1986) [Sov. Phys. JETP **64**, 1075 (1986)].
[5] D. Sánchez and M. Büttiker, Phys. Rev. Lett. **93**, 106802 (2004).
[6] B. Spivak and A. Zyuzin, Phys. Rev. Lett. **93**, 226801 (2004).
[7] J. Wei, M. Shimogawa, Z. H. Wang, I. Radu, R. Dormaier, and D. H. Cobden, Phys. Rev. Lett. **95**, 256601 (2005).
[8] C. A. Marlow, R. P. Taylor, M. Fairbanks, I. Shorubalko, and H. Linke, Phys. Rev. Lett. **96**, 116801 (2006).
[9] R. Leturcq, D. Sánchez, G. Götz, T. Ihn, K. Ensslin, D. C. Driscoll, and A. C. Gossard, Phys. Rev. Lett. **96**, 126801 (2006).
[10] D. M. Zumbühl, C. M. Marcus, M. P. Hanson, and A. C. Gossard, Phys. Rev. Lett. **96**, 206802 (2006).
[11] L. Angers, E. Zakka-Bajjani, R. Deblock, S. Guéron, H. Bouchiat, A. Cavanna, U. Gennser, and M. Polianski, Phys. Rev. B **75**, 115309 (2007).
[12] L. Angers, A. Chepelianskii, R. Deblock, B. Reulet, and H. Bouchiat, Phys. Rev. B **76**, 075331 (2007).
[13] D. Sánchez and M. Büttiker, Phys. Rev. B **72**, 201308(R) (2005).
[14] M. L. Polianski and M. Büttiker, Phys. Rev. Lett. **96**, 156804 (2006).
[15] A. De Martino, R. Egger, and A. M. Tsvelik, Phys. Rev. Lett. **97**, 076402 (2006).
[16] M. L. Polianski and M. Büttiker, Physica E (Amsterdam) **40**, 67 (2007).
[17] A. V. Andreev and L. I. Glazman, Phys. Rev. Lett. **97**, 266806 (2006).
[18] B. Braunecker, D. E. Feldman, and F. Li, Phys. Rev. B **76**, 085119 (2007).
[19] A. Löfgren, C. A. Marlow, T. E. Humphrey, I. Shorubalko, R. P. Taylor, P. Omling, R. Newbury, P. E. Lindelof, and H. Linke, Phys. Rev. B **73**, 235321 (2006).
[20] V. I. Falko and D. E. Khmelnitsky, Zh. Eksp. Teor. Fiz. **95**, 328 (1989) [Sov. Phys. JETP **68**, 186 (1989)].
[21] A. A. Bykov, G. M. Gusev, Z. D. Kvon, D. I. Lubyshev, and V. P. Migal, Pis'ma Zh. Eksp. Teor. Fiz. **49**, 13 (1989) [JETP Lett. **49**, 13 (1989)].
[22] J. Liu, M. A. Pennington, and N. Giordano, Phys. Rev. B **45**, 1267 (1992).
[23] J. J. Lin, R. E. Bartolo, and N. Giordano, Phys. Rev. B **45**, 14231 (1992).
[24] R. E. Bartolo, N. Giordano, X. Huang, and G. H. Bernstein, Phys. Rev. B **55**, 2384 (1997).
[25] A. A. Bykov, Z. D. Kvon, L. V. Litvin, Yu. V. Nastaushev, V. G. Mansurov, V. P. Migal, and S. P. Moschenko, Pis'ma Zh. Eksp. Teor. Fiz. **58**, 538 (1993) [JETP Lett. **58**, 543 (1993)]; A. A. Bykov, L. V. Litvin, N. T. Moshegov, and A. I. Toropov, Super-

lattices Microstruct. **23**, 1285 (1998).
[26] P. W. Brouwer, Phys. Rev. B **58**, R10135 (1998).
[27] T. A. Shutenko, I. L. Aleiner, and B. L. Altshuler, Phys. Rev. B **61**, 10366 (2000).
[28] M. H. Pedersen and M. Büttiker, Phys. Rev. B **58**, 12993 (1998).
[29] P. W. Brouwer, Phys. Rev. B **63**, 121303(R) (2001).
[30] M. G. Vavilov, V. Ambegaokar, and I. L. Aleiner, Phys. Rev. B **63**, 195313 (2001).
[31] J. Q. Zhang, S. Vitkalov, Z. D. Kvon, J. C. Portal, and A. Wieck, Phys. Rev. Lett. **97**, 226807 (2006).
[32] L. DiCarlo, C. M. Marcus, and J. S. Harris, Phys. Rev. Lett. **91**, 246804 (2003).
[33] M. Switkes, C. M. Marcus, K. Campman, and A. C. Gossard, Science **283**, 1905 (1999).
[34] M. Moskalets and M. Büttiker, Phys. Rev. B **69**, 205316 (2004); **72**, 035324 (2005).
[35] M. G. Vavilov, L. DiCarlo, and C. M. Marcus, Phys. Rev. B **71**, 241309(R) (2005) showed that the interference between parasitic rectification and quantum pumping produces current asymmetric to $\Phi \rightarrow -\Phi$ even in noninteracting dot.
[36] C. W. J. Beenakker, Rev. Mod. Phys. **69**, 731 (1997).
[37] I. L. Aleiner, P. W. Brouwer, and L. I. Glazman, Phys. Rep. **358**, 309 (2002).
[38] P. W. Brouwer and C. W. J. Beenakker, J. Math. Phys. **37**, 4904 (1996).
[39] M. L. Polianski and P. W. Brouwer, J. Phys. A **36**, 3215 (2003).
[40] M. Büttiker, A. Prêtre, and H. Thomas, Phys. Rev. Lett. **70**, 4114 (1993); M. Büttiker, J. Phys.: Condens. Matter **5**, 9361 (1993); M. Büttiker, H. Thomas, and A. Prêtre, Z. Phys. B: Condens. Matter **94**, 133 (1994).
[41] P. W. Brouwer, A. Lamacraft, and K. Flensberg, Phys. Rev. B **72**, 075316 (2005).
[42] A. Löfgren, C. A. Marlow, I. Shorubalko, R. P. Taylor, P. Omling, L. Samuelson, and H. Linke, Phys. Rev. Lett. **92**, 046803 (2004).
[43] T. Christen and M. Büttiker, Europhys. Lett. **35**, 523 (1996).
[44] E. P. Wigner, Phys. Rev. **98**, 145 (1955); F. T. Smith, *ibid.* **118**, 349 (1960).
[45] A number of transport problems where the Wigner-Smith matrix plays an important role are reviewed in M. Büttiker and M. L. Polianski, J. Phys. A **38**, 10559 (2005).
[46] P. W. Brouwer, S. A. van Langen, K. M. Frahm, M. Büttiker, and C. W. J. Beenakker, Phys. Rev. Lett. **79**, 913 (1997).
[47] P. W. Brouwer, K. M. Frahm, and C. W. J. Beenakker, Waves Random Media **9**, 91 (1999).
[48] M. L. Polianski, M. G. Vavilov, and P. W. Brouwer, Phys. Rev. B **65**, 245314 (2002).
[49] P. W. Brouwer and M. Büttiker, Europhys. Lett. **37**, 441 (1997).
[50] F. W. J. Hekking and J. P. Pekola, Phys. Rev. Lett. **96**, 056603 (2006).
[51] V. E. Kravtsov and V. I. Yudson, Phys. Rev. Lett. **70**, 210 (1993).
[52] A. G. Aronov and V. E. Kravtsov, Phys. Rev. B **47**, 13409 (1993).
[53] V. I. Yudson, Phys. Rev. B **65**, 115309 (2002).